



Halofuginone-guided nano-local therapy: Nano-thermosensitive hydrogels for postoperative metastatic canine mammary carcinoma with scar removal

Runan Zuo^{a,b,*}, Lingqing Kong^a, Wanjun Pang^a, Shanxiang Jiang^{b,*}

^a Animal-derived food safety innovation team, College of Animal Science and Technology, Anhui Province Key Lab of Veterinary Pathobiology and Disease Control, Anhui Agricultural University, Hefei, Anhui 230036, PR China

^b Engineering Center of Innovative Veterinary Drugs, Center for Veterinary Drug Research and Evaluation, MOE Joint International Research Laboratory of Animal Health and Food Safety, College of Veterinary Medicine, Nanjing Agricultural University, 1 Weigang, Nanjing 210095, PR China

ARTICLE INFO

Keywords:

Thermosensitive hydrogels
Halofuginone
Postoperative
Metastasis
Angiogenesis
Scar removal

ABSTRACT

In female dogs, the highest morbidity and mortality rates cancer are the result of mammary adenocarcinoma, which presents with metastases in the lung. Other than early surgical removal, however, no special methods are available to treat mammary adenocarcinoma. Because human breast cancer and canine mammary carcinoma share clinical characteristics and heterogeneity, the canine model is a suitable spontaneous tumor model for breast cancer in humans. In this study, the physical swelling method was used to prepare halofuginone-loaded D- α -tocopherol polyethylene glycol 1000 succinate (TPGS) polymer micelles nano-thermosensitive hydrogels (HTPM-gel). Furthermore, HTPM-gel was investigated via characterization, morphology, properties such as swelling experiment and *in vitro* release with reflecting its splendid nature. Moreover, HTPM-gel was further examined its capability to anti-proliferation, anti-migration, and anti-invasion. Ultimately, HTPM-gel was investigated for its *in vivo* anticancer activity in the post-operative metastatic and angiogenic canine mammary carcinoma. HTPM-gel presented spherical under transmission electron microscope (TEM) and represented grid structure under scanning electron microscope (SEM), with hydrodynamic diameter (HD) of 20.25 ± 2.5 nm and zeta potential (ZP) of 15.10 ± 1.82 mV. Additionally, HTPM-gel own excellent properties comprised of pH-dependent swelling behavior, sustained release behavior. To impede the migration, invasion, and proliferation of CMT-U27 cells, we tested the efficacy of HTPM-gel. Evaluation of *in vivo* anti-tumor efficacy demonstrates HTPM-gel exhibit a splendid anti-metastasis and anti-angiogenic ability, with exhibiting ideal biocompatibility. Notably, HTPM-gel also inhibited the scar formation in the healing process after surgery. In summary, HTPM-gel exhibited anti-metastasis and anti-angiogenic and scar repair features. According to the results of this study, HTPM-gel has encouraging clinical potential to treat tumors with multifunctional hydrogel.

1. Introduction

The most common tumors in middle-age and elderly female dogs are canine mammary gland tumors (Santos et al., 2023). The malignancy conversion rate of these tumors is approximately 50%. As similar to the type of human breast cancer, canine mammary carcinomas (CMC) can be classified as Adenocarcinoma, Ductular carcinoma, Spindle cell carcinoma, Anaplastic carcinoma, Squamous cell carcinoma, Mucinous carcinoma, Malignant myoepithelioma, Carcinoma or sarcoma in a mixed tumor, Carcinosarcoma (Michishita et al., 2023). Poor clinical indications, such as metastases in the lymph node and lung and high mortality, are associated with the differentiation status of CMC. Like

human breast cancer, CMC has similar characteristics, such as hormonal etiology, age of onset, tumor diversity, stage, lymph node metastasis, and genetic abnormalities (e.g., breast cancer susceptibility gene 2 [BRCA2]) (Zhang et al., 2023b; Chen et al., 2023). Currently, common therapeutic methods of metastatic CMC were surgery and chemotherapy. Whereas there were no specialty chemotherapeutic drugs in the treatment of CMC.

To treat mammary tumors in dogs, the first choice is surgical resection. For inflammatory mammary carcinomas, adjuvant therapy is provided when surgical excision does not enhance quality of life. Chemotherapy, including cyclophosphamide, docetaxel, doxorubicin, and molecular-targeted therapy (e.g., firocoxib, toceranib, and

* Corresponding authors at: Engineering Center of Innovative Veterinary Drugs, Center for Veterinary Drug Research and Evaluation, MOE Joint International Research Laboratory of Animal Health and Food Safety, College of Veterinary Medicine, Nanjing Agricultural University, 1 Weigang, Nanjing 210095, PR China.

E-mail addresses: zrn910314@163.com (R. Zuo), navuy@sina.com (S. Jiang).

<https://doi.org/10.1016/j.ijpx.2024.100241>

Received 1 January 2024; Received in revised form 6 March 2024; Accepted 24 March 2024

Available online 26 March 2024

2590-1567/© 2024 The Authors. Published by Elsevier B.V. This is an open access article under the CC BY-NC-ND license (<http://creativecommons.org/licenses/by-nc-nd/4.0/>).

piroxicam) are offered as adjuvant therapy for CMC (Poirier et al., 2004; Simon et al., 2006; Lavalle et al., 2012; Alonso-Miguel et al., 2022). For labor induction and pyometra treatment, aglepristone, which is an antiprogesterone drug, is administered. Because therapy outcome data are insufficient aglepristone has not been applied in oncology treatment, although its use in dogs with mammary cancers is anticipated (Valdivia et al., 2021). Novel therapeutic strategies are necessary because an adjuvant therapy protocol for CMC (excluding traditional therapy) has not yet been established.

Halofuginone, an orthodox anticoccidial drug, is originated from the Chinese traditional herbs *Dichroa febrifuga* Lour (Lan et al., 2017). Recently, plenty of studies indicated anticancer activity of halofuginone in cancer treatment area especially in breast cancer (Xia et al., 2018). Notably, solid tumors treated with halofuginone was also conducted in a phase I clinical trial. However, halofuginone exhibits several shortcomings such as low solubility, high toxicity, and low bioavailability (de Jonge et al., 2006). To enhance solubility and bioavailability as well as decrease halofuginone toxicity, our previous studies have supported the use of halofuginone-loaded D- α -tocopherol acid polyethylene glycol succinate (TPGS) polymer micelles (HTPM) (Zuo et al., 2021). HTPM also has been shown to impede metastasis in the lung of triple-negative breast cancer compared with halofuginone (Zuo et al., 2022). Nevertheless, HTPM exhibit some deficiencies containing not stable at the tumor site for long periods of time, lower dose at the tumor site. Therefore, searching for a treatment method to improve HTPM is necessary for us.

Promising biomaterials that have a low critical-phase transition temperature include injectable temperature-sensitive hydrogels. These hydrogels will transition from the sol phase to the gel phase if they exceed this critical temperature (Dethe et al., 2022; Hou et al., 2022). To reduce systemic toxicity in normal tissues and maintain use of the injection site as a drug reservoir, temperature-sensitive *in situ* gel has been found to be effective (Liu et al., 2023; Lee et al., 2021). Local chemotherapy with injectable temperature-sensitive gels ensures a high concentration of chemotherapeutic agents is released slowly and consistently at the tumor site, thus increasing its efficiency (Zhang et al., 2021; Wang et al., 2021). In our study, HTPM was added into the thermosensitive gel to prepare the HTPM-gel (Graphical Abstract A). Moreover, HTPM-gel was investigated via morphology, characterization and properties. The capacity for the CMC cell line U-27 (CMT-U27) to migrate, invade, and proliferate has been inspected with use of HTPM-gel and it has been applied to treat recurrent postoperative metastatic and angiogenic CMC (Graphical Abstract B). HTPM-gel was expected to research and develop into a clinical CMC drug for its efficacy reflecting from anti-metastatic, reducing recurrence rates, further contributing to the development of pet medicine.

2. Materials and methods

2.1. Materials and reagents

Shanxi Meixilin Pharmaceutical Co., Ltd. (Yuncheng, China) provided the halofuginone hydrobromide (HF). We purchased D- α -tocopherol polyethylene glycol 1000 succinate (TPGS) from Guangzhou Kafan Biological Technology Co., Ltd. (Guangzhou, China) and poloxamers 188 and 407 from Beiersdorf Biological Technology Co., Ltd. (Hamburg, Germany). Gibco Laboratories (Grand Island, NY, USA) provided fetal bovine serum (FBS). We obtained Roswell Park Memorial Institute (RPMI) 1640 medium, penicillin, trypsin, and streptomycin from Hyclone Laboratories (Logan, UT, USA). We purchased Ki-67, STC-1, VEGF, CD31, BRCA2, TGF- β , Collagen I and Vimentin antibodies and an immunohistochemistry kit from Abcam Biotechnology Co., Ltd. (London, England). We used other chemicals and reagents of analytical grade without further purification.

2.2. Cell line culture

Using RPMI 1640 medium was supplemented with 1% streptomycin, 1% penicillin, and 10% FBS to maintain the CMC cell line CMT-U27 in a cell incubator at 37 °C with 5% CO₂. American Type Culture Collection (Manassas, VA, USA) provided this cell. The normal mouse mammary epithelial line Eph4-ev and canine renal epithelial cell line MDCK were maintained in DMEM supplemented with 1% penicillin, 1% streptomycin and 10% FBS. These two cells were purchased from the Chinese Academy of Sciences Typical Culture Preservation Committee cell bank (Shanghai, China). All cells were cultured in a cell incubator with 5% CO₂ at 37 °C.

2.3. Determination of gelling temperature and gelling time for poloxamer thermosensitive gel solutions

The gelation time was ascertained using a previously established procedure (Agrawal et al., 2020). Poloxamer thermosensitive gel solution (4 mL) stored in the refrigerator at 4 °C was taken and placed in a glass test tube with a thermometer of 0.1 °C accuracy so that the mercury bulb of the thermometer is completely immersed in the gel solution. Furthermore, the test tube was placed in a water bath at 25 °C to make the liquid surface of the water bath 2 cm higher than the gel solution in the test tube. Next, the test tube was set in a water bath at 25 °C, keeping the liquid surface of the bath 2 cm above the gel solution in the test tube, and slowly raising the temperature by 1 °C/min with stirred using a magnetic stirrer at 100 rpm. When the temperature enhanced 0.5 °C, the test tube was tilted 90° to be observed the flow of liquid in the test tube. If the contents of the test tube did not flow, this was defined as gelation of the system and the temperature at that time was the gelation temperature (GT). Three samples were taken from each recipe and the results averaged.

Determining the gelation temperature for the prepared gel was conducted per the established method found in the literature (Altuntas and Yener, 2017). Poloxamer thermosensitive gel solution (4 mL) stored in the refrigerator at 4 °C was taken and placed in a glass test tube with a thermometer of 0.1 °C accuracy for the purpose of the mercury bulb of the thermometer completely immersed in the gel solution. Moreover, the test tube was heated in a water bath at 41 °C, and the liquid level of the water bath was made 2 cm above the gel solution in the test tube. Notably, the timer was started when the temperature of the contents of the test tube was 25 °C. In addition, the test tube was tilted 90° to be observed the flow of liquid in the test tube after a period of time. When gelling occurs in the contents of the test tube, the timing is stopped, and this time is defined as the gelling time. Three samples were taken from each recipe and the results averaged.

2.4. Prescription of halofuginone nano thermosensitive gel (HTPM-gel)

Poloxamer 188 and 407 were added in the ddH₂O according to the proportion of screening (Supplementary Materials Table 1–2) with stirred using a magnetic stirrer at 100 rpm (Supplementary Materials Table 3) to achieve the preparation of poloxamer thermosensitive gel (Blank-gel). Furthermore, the halofuginone-loaded TPGS polymer micelles (HTPM) were prepared via using the method of solvent evaporation. Ultimately, HTPM was added into the Blank-gel with an appropriate volume, which generated the halofuginone nano thermosensitive gel (HTPM-gel).

2.5. Morphology and characterization of HTPM-gel

As-prepared HTPM-gel were further investigated via morphology and characterization. Notably, the exploration of morphology was including surface performance and stereoscopic status. HTPM-gel solution was observed for its surface performance in the condition of 4 °C, 0 min and 37 °C, 1.5 min, respectively. In addition, HTPM-gel was diluted

with deionized water to a suitable concentration and placed onto a 400-mesh copper grid coated with Formva film. Furthermore, HTPM-gel with drying status was laid under a transmission electron microscope (TEM) to examine its size and shape. To inspect the size and shape of the HTPM-gel, which had been frozen for 48 h at $-80\text{ }^{\circ}\text{C}$ and freeze-dried for 48 h at $-60\text{ }^{\circ}\text{C}$, 10 mg of lyophilized powder was taken to view it under a scanning electron microscope (SEM). Alternatively, HTPM-gel solution was diluted with deionized water to a certain concentration, and its hydrodynamic diameter and zeta potential were measured by a nanoparticle analyzer to probe into the characterization of HTPM-gel. Finally, sufficiently dried HTPM-gel samples were mixed with potassium bromide (mass ratio 100:1–150:1) and ground into powder, pressed into tablets and then the characteristic absorption peaks of the chemical groups were determined using Fourier Transform Infrared spectroscopy (FTIR) (Shimadzu Instruments Co., Ltd., Kyoto, Japan). Meanwhile, Blank-gel and HTPM-gel were researched using X-ray diffraction (XRD; D8 Advance, Bruker-AXS, Karlsruhe, Germany) to analyze two hydrogels structure changes during the formation process. Further, the aforementioned samples were placed in a crucible and compacted on a glass slide. Subsequently, XRD equipped with a Cu/K α radiation source was performed at $4^{\circ}/\text{min}$ in the scanning range of 5° – 50° under the conditions of 40 kV/40 mA.

A PerkinElmer Calorimeter Pyris 1 with nitrogen were used as a purge gas to take differential scanning calorimetry (DSC) measurements. Indium, water, and zinc standards were used to calibrate the calorimeter. Thermogravimetric analysis (TGA) of Blank-gel and HTPM-gel was performed by using differential scanning calorimeter (model: DTG 500; Shimadzu Corporation, Kyushu, Japan). All samples were subjected to heating between $25\text{ }^{\circ}\text{C}$ and $300\text{ }^{\circ}\text{C}$ at a heating rate of $10\text{ }^{\circ}\text{C}/\text{min}$ and 30 mL/min. Three different samples were selected from the same batch to repeat measurements and verify reproducibility. Ultraviolet (UV) spectrophotometry (UV-1900; Shimadzu Instruments (Suzhou) Co., Ltd.) was used in the wavelength between 200 and 800 nm to analyze the UV spectral absorption spectra of the HTPM-gel.

2.6. Determination of phase change temperature

The hydrogel was placed in equilibrium in a test tube, and then we added 10 mL of water into the tube. A thermometer was inserted and then warmed up the test tube in a water bath at constant temperature. Further, the change in volume of the hydrogel with temperature is measured to determine the temperature at which the volume of the hydrogel should expand to contract. The hydrogel underwent a reversible discontinuous volume change from hydrophilic to hydrophobic as a result of small changes in temperature (called the lower critical solution temperature [LCST]).

2.7. Swelling experiments and syringeability test of HTPM-gel

Distilled water (for analyzing the swelling and deswelling rates of hydrogels at different time points) and pH 1–12 PBS solution (for investigate the swelling rate of hydrogels at different pH conditions) were respectively used in closed containers at $37\text{ }^{\circ}\text{C}$ to analyze swelling experiments of HTPM-gel. The swollen samples were removed at specific time intervals. Then, soft paper was used to blot the surface, weighed the samples, and returned them to the solution until we achieved equilibrium weight.

The following formula was used to calculate the swelling ratio:

$$\text{Swelling Ratio (SR)} = (W_s - W_d)/W_d, \quad (1)$$

where W_d and W_s are the weight of the hydrogel samples in dry and swollen states, respectively.

The hydrogels were vacuum dried to a constant weight and swollen with deionized water at $25\text{ }^{\circ}\text{C}$ for 24 h, then the surface was dried to determine the mass and the equilibrium swelling rate was calculated.

After deionized water was used at $25\text{ }^{\circ}\text{C}$ to enable the hydrogel to reach swelling equilibrium, the swollen hydrogel was rapidly transferred to deionized water at $100\text{ }^{\circ}\text{C}$. At this point, the hydrogel shrank and lost water to reach a status of de-swelling. The mass of the hydrogel (W_t) is measured at regular intervals until it no longer changes.

The water retention (WR) was calculated using following formula (2):

$$\text{WR (\%)} = 100 \times (W_t - W_d)/W_s \quad (2)$$

Water retention with time curve was made to obtain the kinetics of the hydrogel at $100\text{ }^{\circ}\text{C}$.

Injectability of hydrogels makes it easier to inject for better therapeutic results. HTPM-gel were filled into 1 mL plastipak syringes and stored at $4\text{ }^{\circ}\text{C}$ for 12 h. They were kept at $25\text{ }^{\circ}\text{C}$ at least 10 min before measurement. Three different needles with their respective specifications such as 27G (0.19; 20 mm), 29G (0.16; 88 mm), and 30G (0.14; 13 mm) were to perform syringeability experiments on HTPM-gel at $25\text{ }^{\circ}\text{C}$. Herein, the displacement rate of the plunger was 0.5 mm/s , which was similar to a manual injection rate: $0.4\text{ mL}/\text{min}$. Needle characteristics was examined including diameter and length, as well as HTPM-gel concentrations between 0 and 60 mM, affected injection force. All measurements were performed in triplicate at $25\text{ }^{\circ}\text{C}$ on each gel.

2.8. In vitro release profiles

The in vitro release behavior of HTPM (pH 6.5) and HTPM-gel (pH 6.5) was studied by the dialysis bag method. The release performance of hafuginone in the HTPM was conducted out in accordance with method of the previous study (Zuo et al., 2021). 50 mg of HTPM-gel was placed into a PBS solution. 500 mL of the PBS solution was dialyzed under consistent shaking at 100 rpm at $37 \pm 0.5\text{ }^{\circ}\text{C}$. After withdrawing 5.0 mL of release medium at scheduled times and it was replenished with 5.0 mL fresh buffer medium. We used a UV-vis spectrophotometer (UV-1900; Shimadzu Instruments (Suzhou) Co., Ltd.) to record the amount of hafuginone released at 243 nm in the HTPM and HTPM-gel. Above experiments were carried out in triplicates ($n = 3$).

2.9. Cell viability assay evaluation of hydrogels in vitro

The in vitro cytotoxicities of Blank-gel and HTPM-gel were evaluated by a Cell Counting Kit-8 (CCK-8, KeyGen Biotech Co., Ltd., Nanjing, China). CMT-U27 cells (5×10^3 cells per well) were seeded into a 96-well plate overnight, and then treated with Blank-gel and HTPM-gel at a range of concentrations (0–50 nM). Prior to the incubation endpoint, CCK-8 reagent (10 $\mu\text{L}/\text{well}$) was added to each well and incubated at $37\text{ }^{\circ}\text{C}$ for 1 h, after which the optical density was determined at a wavelength of 450 nm. Untreated cells were used as controls, cell viability was calculated according to the following formula (3):

$$\text{Cell viability (\%)} = (\text{OD}_{\text{treated}} - \text{OD}_{\text{blank}}) / (\text{OD}_{\text{untreated}} - \text{OD}_{\text{blank}}) \times 100\% \quad (3)$$

2.10. In vitro biocompatibility of hydrogels

Eph-ev cells and MDCK cells were used to detect the biocompatibility of the hydrogels through the CCK-8 kit assay. 5×10^3 cells/well of Eph-ev cells and MDCK cells were seeded into 96-well plates and then treated with Blank-gel and HTPM-gel at a range of concentrations (0–50 nM). After incubation for 24 h, CCK-8 solution was added and incubated for 1 h, and the cell absorbance was detected at 450 nm by a microplate reader. Cell viability was calculated according to the following formula (3).

2.11. Colony-formation assay

A colony formation assay was used to inspect the colony-forming ability of CMT-U27 cells. After seeding CMT-U27 cells (1×10^3 cells

per well) in a six-well plate, they were incubated overnight. Further, CMT-U27 cells were pretreated with Blank-gel (5 nM) and HTPM-gel (5 nM), respectively. Every two days, the culture medium was refreshed and observed colony formation. The clones were fixed in cell plates with paraformaldehyde (4%) for 5 min after the control cells had formed large clones. Then 0.5% crystal violet (1 mL) was added to each well and stained the cells for 10 min. Then 0.5% crystal violet was removed with pure water. Colony formation was taken photographs and used Image J software (National Institutes of Health, Bethesda, MD USA) to quantify the numbers of cell clones in the obtained colony images. All the experiment were replicated for 3 times.

$$\text{Colony formation rate} = (\text{Counts of clones} / \text{Number of cells inoculated}) / 100\% \quad (4)$$

2.12. Wound-healing assay

Following the method described previously in (de-Oliveira et al., 2015), a wound-healing assay was conducted. The CMT-U27 cells were seeded into six-well plates at a density of 5×10^5 /cell and cultivated the cells to convergence. Using a sterile 100 μ L disposable micropipette tip, a straight-line scratch was established and then they were washed twice with PBS to remove debris. At three processing times (0, 12, and 24 h), the fresh serum-free medium was replaced with contained Blank-gel (5 nM) and HTPM-gel (5 nM). An inverted phase-contrast microscope (Leica, Wetzlar, Germany) was used to photograph the microscopic scratch wound area from each plate. The experiments were repeated three times each.

2.13. Transwell invasion assay

To conduct transwell invasion, CMT-U27 cells (2×10^4 cells per well) was placed in Matrigel-coated (Corning Incorporated, Corning, New York, USA) upper chambers (serum-free medium is used as upper culture medium, and 0.05–0.2% bovine serum albumin (BSA) may be added to maintain osmotic pressure), which were then resuspended with Blank-gel (5 nM) and HTPM-gel (5 nM). The medium plus 10% FBS was added as the chemo-attractant to the lower chamber. After 24 h incubation, any cells that had not invaded the membrane were removed. After the cells were fixed on the surface of the bottom chambers with 4% paraformaldehyde, they were stained with 0.5% violet. An inverted phase-contrast microscope (Leica) was used to count and photograph the cells in microscopic fields. All the experiment were replicated for 3 times.

2.14. Animal experiments

Four-week-old female BALB/c nude mice was purchased from the Comparative Medicine Laboratory Animal Center of Yangzhou University (Yangzhou, China). The mice were raised in Nanjing Agricultural University's (NJAU) Laboratory Animal Center and experiments were performed following the NJAU Guidelines for Animal Experimentation. The NJAU Animal Ethics Committee approved the research protocols for the orthotopic CMC xenograft models (No. 20211224203).

2.15. Establishment of postoperative orthotopic CMC mice

To establish the orthotopic or CMC mouse models, we injected CMT-U27 cells (1×10^6 cells/mouse) into the second pair of mammary glands on the right. Vernier calipers were used to measure the length and width of the tumors and we calculate the tumor volume using the formula $V = (a \times b^2) / 2$, where a and b represent the tumor's longest length and its relatively shorter width, respectively. The tumors were surgically resected on a sterile operating table once the tumor measured 80–100 mm³. Following the process in a previous study, the surgery and post-operative suture was complete (Chen et al., 2019).

2.16. Treatment effect of HTPM-gel on postoperative orthotopic CMC mice

15 mice were randomly divided into four groups to undergo surgical resection as follows: (1) tumor resection surgery (TRS), (2) TRS + Blank-gel, and (3) TRS + HTPM-gel. Every two days on days 0–14, the nude mice were orthotopically injected with the same volume of Blank-gel, HTPM-gel. Every two days until day 15, the tumor size was measured and body weight for each mouse. The mice were dissected and collected the main organs, including heart, liver, spleen, lung, and kidney, and tumor tissues for immunohistochemical or pathological analysis at the end of the experiment. TUNEL staining was utilized to detect the apoptosis of tumor tissues and Image J was used to count and calculate the apoptosis rate of tumor tissues in each group, which indicated estimate the % of necrosis degree in the tumor samples (Tan et al., 2021). A Blood Cell Analyzer (Mindray, Shenzhen, China) was used to evaluate the biochemical representative and blood physiological indices, including haematoblast (HGB), glutamic-pyruvic transaminase (ALT), glutamic oxaloacetic transaminase (AST), lymphocyte (LYMPH), monocyte (MONO), and neutrophil (NEUT). Immunohistochemical analysis was conducted using Image J to determine the optical density value and relative expression level of the representative indicators of tumor proliferation and metastasis (e.g., STC-1 and BRCA2). To measure interleukin-17 (IL-17) and interleukin-22 (IL-22), commercial cytokines kits were used with independent instructions (BioLegend). VEGF, CD31, ki-67 and vimentin were determined to detect the effect of HTPM-gel on angiogenesis, neovascularization, proliferation and epithelial mesenchymal transformation (EMT) of tumor tissue via immunohistochemistry and real-time quantitative PCR.

2.17. Efficacy of HTPM-gel on scar removal from postoperative orthotopic CMC mice

To investigate the efficacy of HTPM-gel on scar removal from post-operative in situ CMC mice, scar in the surgical site were observed by the camera, with relative indicators such as TGF- β and Collagen I determined via the immunohistochemical analysis for each group from excision of wound granulation tissue or scarred skin from healed wounds. Blood samples were collected and coagulated for 30 min at 25 °C after the experiment ended. Serum was then collected after centrifugation at 15,000 g for 15 min. IFN- γ and TNF- α were detected using ELISA MAX Deluxe mouse IFN- γ and TNF- α kits. (Bio Legend), respectively.

2.18. Statistical analysis

To conduct data analysis, we used GraphPad Prism 6.0 (La Jolla, CA, USA). To evaluate between-group differences we used Student's *t*-test. Data are given as the mean \pm standard deviation (M \pm SD). To determine significant differences, analysis of variance (ANOVA) multiple comparison tests were performed, including Bonferoni's and Tukey's tests, and considered **P* < 0.05, ***P* < 0.01, and ****P* < 0.001 to be statistically significant, statistically extremely significant, and statistically the most significant, respectively.

3. Results

3.1. Preparation of HTPM-gel

Preparation of HTPM-gel was carried out according to the physical swelling method (Fig. 1A). Firstly, the proportion of poloxamer 407 and poloxamer 188 was screened out via certain gelation temperature and gelation time which were in accordance with pet dogs (Supplementary Materials Table 1–2). Then, the poloxamer 407 (9 g) and the poloxamer 188 (2 g) of system volume were added into distilled water (40 mL), which was defined as the poloxamer thermosensitive gel (Blank-gel).

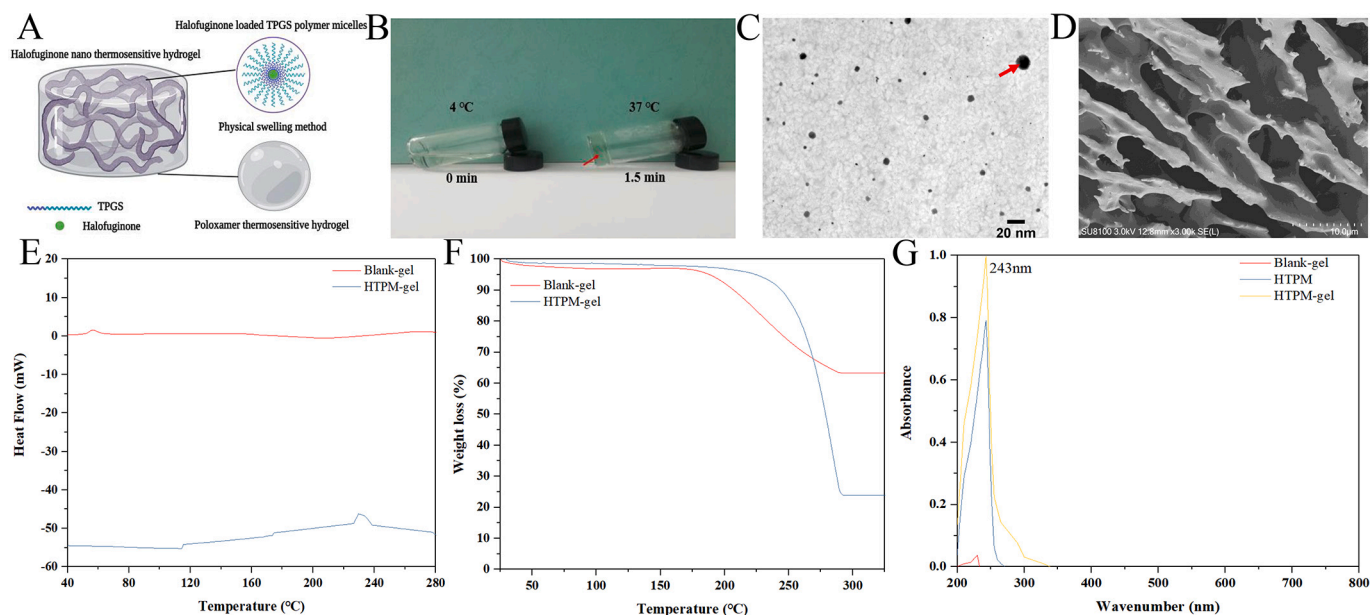


Fig. 1. Characterization and morphology of the HTPM-gel. (A) The HTPM-gel was prepared via a physical swelling method. (B) Physical morphology of the HTPM-gel showed the solution status at 4 °C and the gel status at 37 °C after 1.5 min, which indicated the temperature sensitivity of the HTPM-gel. (C) We used transmission electron microscopy to observe the surface morphology of the HTPM-gel. (D) We used scanning electron microscopy to observe the surface morphology of the HTPM-gel. (E) (Differential Scanning Calorimetry) DSC analysis of HTPM-gel in situ gel depot samples were investigated via differential scanning calorimetry, $n = 3$. (F) Thermogravimetric analysis (TGA) of HTPM-gel in situ gel depot samples were determined by a thermogravimetric analyzer, $n = 3$. (G) The UV absorption spectrum indicated that the HTPM-gel had the largest characteristic absorption peak at 243 nm ($n = 3$).

Finally, 400 μL of HTPM was added into the Blank-gel to promote the formation of HTPM-gel.

3.2. Morphology and characterization of HTPM-gel

With the aim of exploring the nature for halofuginone nano thermosensitive hydrogel, the morphology and characterization were further investigated. Briefly, the morphology of HTPM-gel was inspected via surface performance and three-dimensional shape. As for surface performance, the as-prepared HTPM-gel exhibit thermosensitive characteristics from the liquid status at 25 °C into hydrogel state at 37 °C (Fig. 1B and Fig. S1A, B). Transmission electron microscope (TEM) was used to observe the morphology of HTPM-gel and found that the HTPM-gel had a spherical structure about 20 nm in length, indicating structural stability (as shown in the Fig. 1C). Furthermore, there are no aggregation in the HTPM-gel, which demonstrated the uniform distribution. Notably, the stereoscopic morphology of HTPM-gel was characterized using scanning electron microscope (SEM) after a lyophilization process. According to SEM, because of additional crosslinking between HTPM and Blank-gel networks, the hydrogel-bearing HTPM showed tight and uniform nanofibrous intertwining structures at pH 7. In addition, because of crosslinking between HTPM and poloxamer hydrogel networks, the HTPM-gel revealed a grid structure (Fig. 1D). Notably, to prevent the HTPM from leaking out of the hydrogel into an aqueous solution, it could be fixed on the networks.

The characterization of HTPM-gel was investigated in regard to its zeta potential (ZP) and hydrodynamic diameter (HD). HD of HTPM-gel was observed as a value of 20.25 ± 2.5 nm with PDI of 0.218 ± 0.015 , which indicated that the nanoparticle size distribution was uniform (Fig. S2A and Table S4). Alternatively, HTPM-gel owned a small peak about 20.6 nm in the left of main peak, which demonstrated the HTPM-gel exhibited a smaller particle size and can further penetrate into tumor tissue and cells with its higher permeability (Zhang et al., 2020). Also demonstrating high homogeneity, the PDI of HTPM was 0.231 ± 0.2 and the ZP of HTPM was 14.40 ± 0.1 mV, according to a recent study (Zuo et al., 2021). The mutual repulsion between particles

was better and the system was stable as reflected in the positive charge of the HTPM-gel, which had a ZP of 15.10 ± 1.82 mV (Fig. S2B and Table S4) (Augustine et al., 2020). The DSC thermogram of Blank-gel and HTPM-gel is presented in Fig. 1E. The DSC curves of Blank-gel revealed a wide exothermic peak at approximately 60 °C owing to a decrease in the moisture content of poloxamer 407. A wide endothermic peak was observed in the DSC curve of HTPM-gel in the range of 100–120 °C. This peak indicated that the thermo-responsive monomer decomposed at higher temperatures. An exothermic peak was also observed at 220–240 °C that suggested the existence of HTPM. As depicted in Fig. 1F, the starting loss of weight for Blank-gel began at a decomposition temperature range of 60–175 °C, which was connected to the entrapped water evaporation after which there was full rapidly degradation. Interestingly, the thermal stabilities of the HTPM-gel were characterized using TG analysis at 20–325 °C in an N₂ atmosphere. Moreover, according to the recorded thermograms, HTPM-gel revealed the first weight loss at a decomposition temperature (Td) of about 50 °C, likely due to the release of absorbed moisture. At roughly 200 °C, a second abrupt degradation peak was also noted in the thermogram of HTPM-gel at Td. This peak indicated the release of moisture and entire weight loss that had been trapped. In addition, previous studies manifested micelles incorporated into hydrogel can enhanced its thermal stability (Rocha et al., 2022). Thus, above results indicated HTPM-gel have an excellent thermal stability. Furthermore, HTPM-gel has a maximum absorption wavelength at 243 nm with similar to maximum ultraviolet absorption spectrum of HTPM, as detected by UV absorption spectroscopy which demonstrated the HTPM successfully incorporated in the Blank-gel to prepare the HTPM-gel (Fig. 1G).

FTIR showed that the HTPM-gel had characteristic absorption peaks of C—H, C—O, C—X, C—C, $\sigma\text{C—H}$ at 2885, 1468, 1343, 1283, 1107, 964, and 842 cm^{-1} (Fig. S3B). Notably, Blank-gel has a saturated C—H stretching vibration peak at 2896 cm^{-1} , whereas the C—H of HTPM-gel is shifted, suggesting that the addition of HTPM into Blank-gel has made HTPM-gel more stable. Interestingly, HTPM has a C—X stretching vibration peak at 1272 cm^{-1} , whereas there is no C—O stretching vibration peak at 1283 and 1243 cm^{-1} . Moreover, HTPM-gel have C—O peaks at

1283 and 1243 cm^{-1} , while the C-X (halogen) peak disappears at 1272 cm^{-1} , which indicated that HTPM was successfully dissolved in Blank-gel via physical swelling methods to obtain HTPM-gel. As depicted in the Fig. S3A, the X-ray diffraction pattern of the blank gel included multiple strong diffraction peaks, indicating a gel structure. These peaks were still observed in the HTPM-gel, which further demonstrated HTPM was successfully dissolved in Blank-gel to acquire HTPM-gel.

3.3. Swelling experiments and syringeability test of HTPM-gel

HTPM-gel can reach the swelling equilibrium after about 24 h at 37 °C, and the swelling rate increased for a while then remained unchanged (Fig. 2A). The reason for the increase in the swelling rate of HTPM-gel is that the longer the dry hydrogel immersed in the secondary water, the more hydrogen bonds will be destroyed. The macroscopic aspect is that the swelling ratio becomes larger than previous results. After 4 h, HTPM-gel can reach the swelling equilibrium, have different degrees of decline in the initial stage, and tend to equilibrium in the end (Fig. 2B). Because of the hydrogen bond between the water molecule and the hydrophilic group, the hydrogel had better water absorption properties with the hydration layer of the hydrophobic group when the temperature was lower than 37 °C (the LCST of gel).

Meanwhile, the hydrogel had to be squeezed out owing to the appearance of numerous free water molecules, resulting in a decrease in the swelling rate and poor water absorption. Furthermore, the deswelling rate is independent of the diffusivity of free water through the gel network structure, which is controlled by the diffusivity and the gel morphology. In the initial stage of swelling, the hydrogel undergoes a phase transition if the temperature is higher than the critical temperature. In the meantime, the large area of the gel surface shrinks, which causes a dense, thick shell layer to form (Torres-Figueroa et al., 2021).

As depicted in the Fig. 2C, the swelling rate of the hydrogel increased initially and then decreased with the diverse pH condition. Interestingly, the group RCOCHNH₂ on the hydrogel was more positively charged and became RCOCHNH₂⁺ under acidic conditions, with the electrostatic repulsion between molecular chains enhanced, further led to an increase in the swelling rate of the gel. Alternatively, the part of

RCOCHNH₂ on the hydrogel was negatively charged and altered into RCOCHN⁻ under alkaline conditions, and the electrostatic repulsion between molecular chains was enhanced, resulting in the swelling of the gel. Nevertheless, the osmotic pressure outside the gel gradually tends to zero as time goes on. More importantly, the general molecular formula of poloxamer is HO—(C₂H₄O)_a—(C₃H₆O)_b—(C₂H₄O)_c—H, where values of a and c are 2–130 with value of b is 15–67. 2.5% poloxamer aqueous solution has a pH between 5.0 and 7.5, and its water for injection has a pH between 6.0 and 7.0. In addition, poloxamer is more likely to acquire a positive charge and take on a positive charge owing to its phenolic hydroxyl group (De et al., 2023). HTPM-gel exhibit pH sensitivity may contribute to its chemical structure reflected from those characteristic functional group such as phenolic hydroxyl group (weak acid group), which focused on the ionization of functional groups under different pH conditions. The dissociation of functional groups in HTPM-gel increased with increasing pH under acidic conditions, while the solubility enhanced.

In addition, the injectability of HTPM-gel was measured (Figs. 2E-F). For subcutaneous administration, it is required that colloids are injectable at room temperature (25 °C). The injection force was measured via using the three needles, which was below 10 N (Fig. 2E). If the needle's diameter was larger (29G vs. 30G), when the needle was longer, the injection force was higher. In contrast, at 30 mM, the HTPM-gel showed the highest injection force (Fig. 2F).

3.4. In vitro release files of halofuginone from HTPM and HTPM-gel

To increase drug bioavailability for tumor therapy, controlled and sustained release is critical. We followed the dialysis bag method to determine the halofuginone release profiles from HTPM and HTPM-gel in PBS with pH 6.5 (Fig. 2D). Typically, in the CMC microenvironment, pH usually is close to 6.5 (Deng et al., 2020). Within 24 h, under this pH environment, the CRP of halofuginone from HTPM rose to 64.48%. Weakly acidic environments thus improved the HF release rate from HTPM, demonstrating that it would be beneficial for treating cancer cells that are acidic. The low blood concentration and fast distribution reflect the pharmacokinetic properties of free halofuginone. Pharmacokinetic studies of free halofuginone by intraperitoneal, oral,

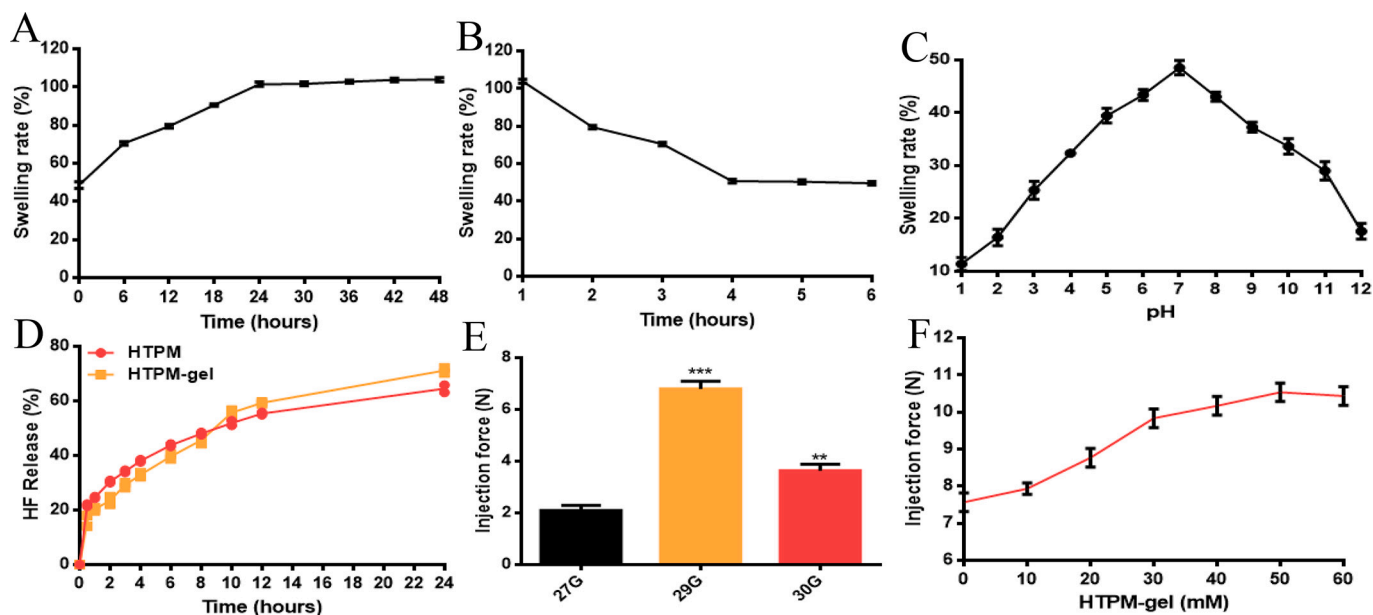


Fig. 2. Properties of the HTPM-gel. (A) Swelling rate and (B) de-swelling rate of HTPM-gel were investigated at various time via determination of weight change in dissolved hydrogels, $n = 3$. (C) Swelling rate of HTPM-gel were explored by different pH conditions, $n = 3$. (D) Using the dialysis bag method, we investigated the in vitro drug release HF profiles of the HTPM and HTPM-gel in a PBS solution (pH 7.2–7.4) ($n = 3$). (E) We used 27G, 29G, and 30G needles to measure the maximal injection force for HTPM-gel ($n = 3$). (F) We used a 29G needle to measure variations in injection force as a function of HTPM-gel concentration ($n = 3$).

and intravenous injection have been reported (de Jonge et al., 2006). Remarkably, the CRP of halofuginone from HTPM-gel were approximately 71.18% within 24 h, indicating that HTPM-gel have sustained release effect in comparison with HTPM, further demonstrating HTPM-gel enhanced tumor accumulation and penetration abilities and prolonged tumor retention abilities (Hammad et al., 2020). Alternatively, HTPM-gel exhibited more excellent slow-release effect compared to other halofuginone hydrogels, which further highlighted the advantages of the developed system in this article (Sassi et al., 2018). As mentioned previously, hydrogels can be able to form a three-dimensional network structure with large pores and surface area, which can effectively carry and release drugs compared with other drug delivery systems (Ali et al., 2024). This high drug-carrying capacity improves drug loading and release efficiency. The structure of hydrogels can be modulated to achieve precise control of drug release. By adjusting the composition of the hydrogel, the degree of cross-linking, pore size and other parameters, slow release can be achieved to meet different therapeutic needs (Touzout et al., 2024).

3.5. Enhanced treatment effect of HTPM-gel toward CMT-U27 cells

Colony formation assay was used to explore the anticancer ability of HTPM-gel to treat CMC-U27 cells. CMT-U27 cell viability decreased

significantly after 24 h or HTPM-gel treatment versus Blank-gel treatment (Fig. 3C). According to the statistical analysis, HTPM-gel was also better able to suppress colony formation against CMT-U27 cells than Blank-gel (Fig. 3D). In addition, as depicted in the Fig. S4A, HTPM-gel was also better able to suppress the proliferation of CMT-U27 cells compared with Blank-gel. Therefore, these results showed that the HTPM-gel demonstrated stronger anticancer activity than Blank-gel. Alternatively, HTPM-gel exhibited a prominent biocompatibility which reflected from the results of Figs. S4B–4C. In brief, HTPM-gel have higher security for Eph4-ev cells and MDCK cells.

3.6. Invasion and migration of CMT-U27 cells inhibited by HTPM-gel

A major malignant feature of CMC is tumor metastasis, which causes >90% of deaths related to CMC (Li et al., 2023). In diseased dogs, a prospective strategy to enhance survival rates is the efficient suppression of tumor metastases. In this study, the effect of HTPM-gel was evaluated on the invasion speed of CMT-U27 cells using a wound-healing assay. The HTPM-gel more effectively inhibited the migration of CMT-U27 cells than the Blank-gel in a time-dependent manner style (Fig. 3A, B). To demonstrate the effect of HTPM-gel on the invasion and migration of tumor cells, we also applied the transwell assay. In the Blank-gel-treated groups, we found that the invasion and migration of cancer cells was

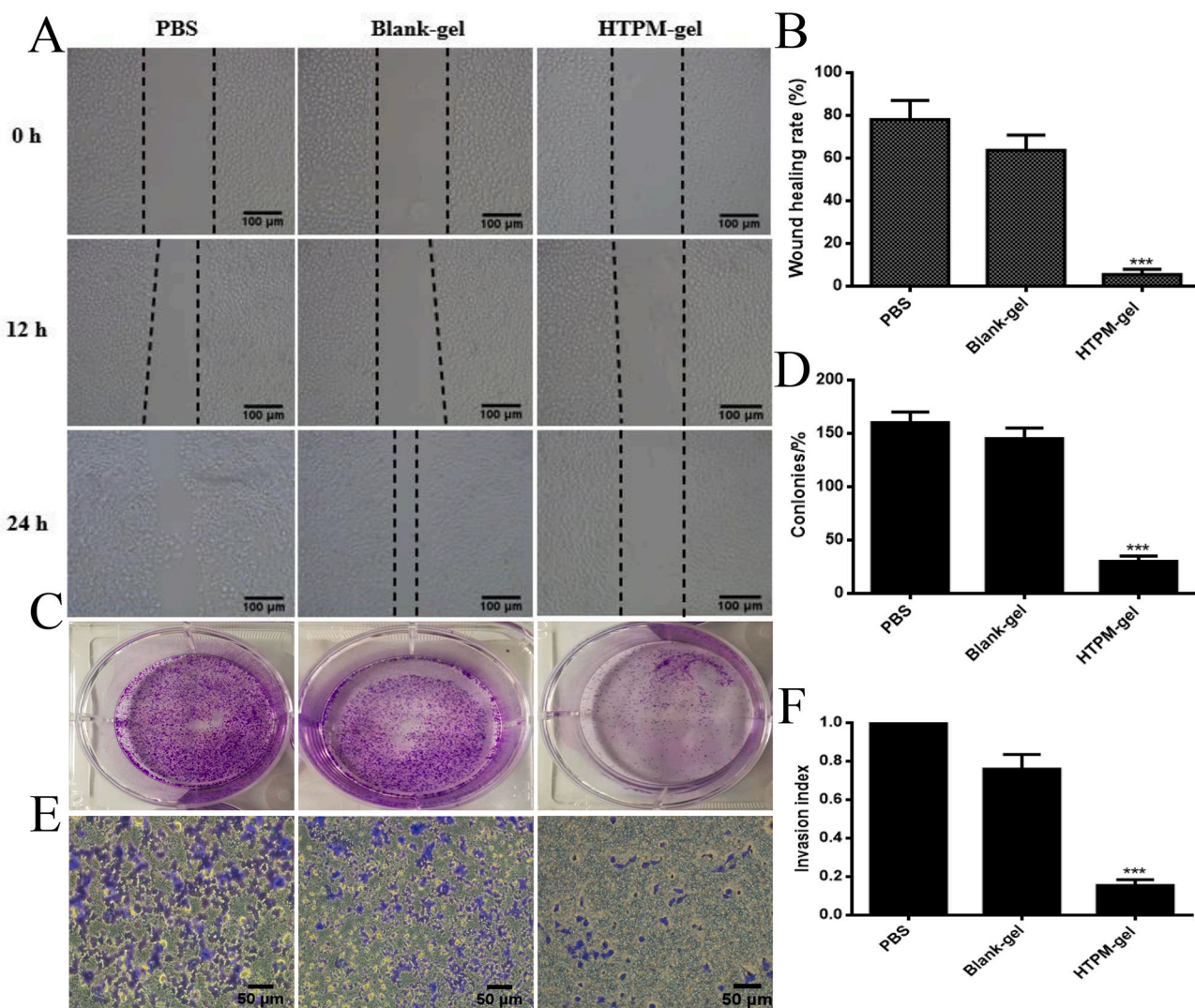


Fig. 3. The impact of the HTPM-gel on migration, clone formation, invasion activity for CMT-U27 cells. The HTPM-gel significantly inhibited migration (A&B), (C&D) clone formation, and (E&F) invasion of CMT-U27 cells compared with PBS and Blank-gel (n = 3).

extensive but the migration and invasion of CMT-U27 cells was impeded by HTPM-gel (Fig. 3E, F). In HTPM-gel, fewer CMT-U27 cells invaded and migrated into the bottom chamber than in Blank-gel. HTPM-gel also demonstrated better inhibition of cell invasion than Blank-gel (Fig. 3E, F). According to results, HTPM limited tumor cell invasion in a manner that was concentration dependent.

3.7. *In vivo* growth of CMC restricted by HTPM-gel

To further evaluate the *in vivo* growth ability of CMC tumor tissue impeded by HTPM-gel, vernier calipers and HE staining techniques were applied to investigate the proliferation of various groups (Boix-Montesinos et al., 2021). We in situ injected CMT-U27 cells into the right second pair mammary of BALB/C nude mice (Fig. 4A). Surgery resection was used to remove 80–90% of the tumor tissue once tumor volume reached 80–100 mm³. After pre-treatment of drug administration, Blank-gel and HTPM-gel were orthotopically administrated at the same volume (100 μL) per two days until the experiment end. Interestingly, body weight in diverse group remained relatively stable and stayed within a range from 18 to 24 g, which indicated these hydrogels have excellent safety (Fig. 4B). Further, tumor volumes were significantly decreased in the HTPM-gel (76.84% ± 1.32%), whereas that of Blank-gel treatment was only 3.57% ± 1.03% (Fig. 4C), and these results were demonstrated via observations of tumor morphology from Fig. 4D. On day 14, we killed the mice, collected tumor samples by dissection,

and took photographs (Fig. 4D). In the Blank-gel-treated groups, the tumor weights were much higher than those in the HTPM-gel-treated group (Fig. 4E). Like the subcutaneous CMC treatment by gavage, the H&E staining of orthotopic tumor sections showed that HTPM-gel-treated tumor samples had more necrosis than those in the Blank-gel-treated groups. Notably, the maximum amount of necrosis persisted in tumors from the HTPM-gel-treated group (Fig. 4F and Fig. S5). Furthermore, TUNEL staining of tumor tissues clearly showed significant apoptosis induced by HTPM-gel compared with other treatments. As depicted in the Fig. 4G, HTPM-gel significantly induced apoptosis in tumor tissue (68 ± 1.41%) compared with Untreated (4.67 ± 1.52%) and Blank-gel group (5.33 ± 1.53%). All these results strongly suggested that HTPM-gel hold effective tumor inhibition capability, tumor accumulation and penetration abilities and prolonged tumor retention abilities.

3.8. Metastasis of CMC impeded by HTPM-gel

To confirm the antitumor mechanism of HTPM-gel, we examined vessel density (lymphatic and blood vessel) and VEGF signaling in the tumor region. The HTPM-gel-treated tumors had an obviously higher blood vessel density than the Blank-gel group, which we visualized by anti-CD31 immunohistochemistry, as well as higher VEGF expression as a result of hypoxia-induced angiogenesis (Xia et al., 2019). The vessel density and VEGF levels were significantly reduced in the tumor tissue

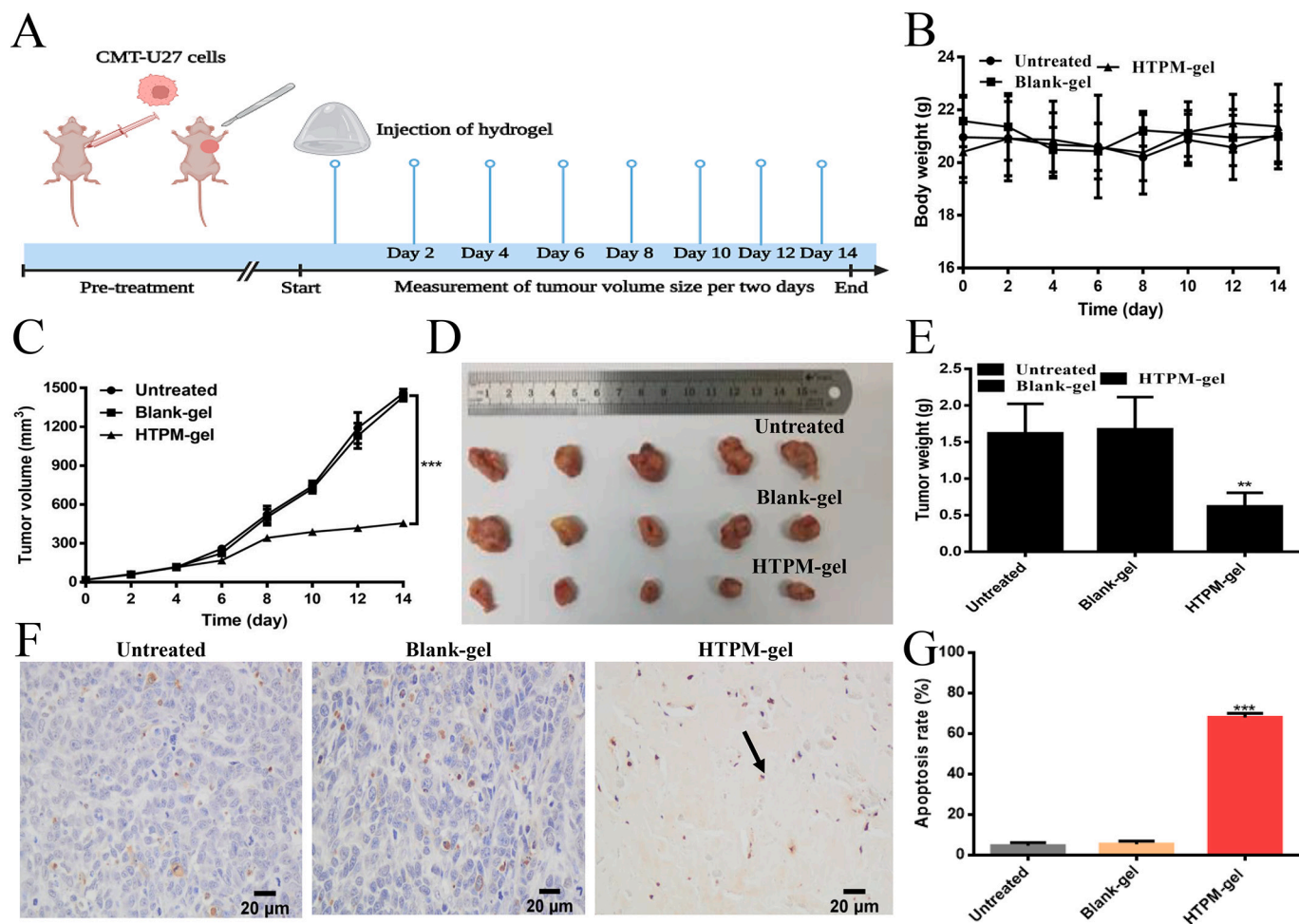


Fig. 4. HTPM-gel administrated in situ had anticancer effects against postoperative orthotopic CMC xenografts in nude mice. (A) Pattern diagram, (B) body weights, (C) tumor volumes, (D) morphology of the harvested tumors, (E) tumor weights, and (F) TUNEL staining analysis (400×) of the degree of tumor necrosis and apoptosis rates (G) for drug-untreated nude mice or after administration of the Blank-gel, HTPM-gel (n = 5). The tumor images of the HTPM-gel are shown in black arrows, which indicate apoptosis of the tumor tissue induced from HTPM-gel. **P* < 0.05, ***P* < 0.01, ****P* < 0.001.

treated with HTPM-gel (Fig. S6). This result showed that HTPM-gel neutralized the response of angiogenic tumors to hypoxia and also enhanced combinatory cancer therapy. Furthermore, this result was demonstrated via RT-Q-PCR technique (Fig. S7 and Table S5). Compared with Blank-gel, HTPM-gel significantly inhibited the expression of VEGF and CD31. For several decades, how angiogenesis affects tumor growth has been a focus of research, and it is now understanding that angiogenesis is necessary for establishment and migration of tumor metastases.

As an anti-angiogenic agent, it is possible that HTPM-gel prevents tumor metastasis through the anti-angiogenesis pathway and by collaborating with the hypoxia-inducible hydrogel to optimize HTPM-based chemotherapy. The *in vivo* therapeutic outcomes have been encouraging. Thus, an orthotopic CMC tumor model was used to evaluate the anti-metastasis ability of HTPM-gel. The significant enhancement in the enhanced tumor inhibitory effect of HTPM-gel was attributed on the synergy of HTPM-based chemotherapy. Lymphatic vessel and tumor blood growth are key factors for tumor hematogenous metastasis (Urner et al., 2019). As a result of hydrogel exposure to specifically block the expression of VEGF, halofuginone was released. In this study, we expected that this association with vascular growth would inhibit the lymphatic and blood vascular growth for mitigating tumor hematogenous metastasis. Therefore, we extracted the lungs of mice following therapy for histological analysis to count and verify HTPM-gel's anti-metastasis effect. The H&E staining images showed no tumor metastasis in the lungs of mice following HTPM-gel-mediated therapy (Fig. 5); after other treatments, however, metastatic tumors were distributed in the lungs of mice. Tumor parenchymal cells was also observed in pathological slides of the lung of mice in the PBS-injected control and Blank-gel injected groups. In HTPM-gel-treated mice, we

did not count any tumor parenchymal cells with pulmonary metastasis nodules. Furthermore, lung metastasis related pivotal protein STC-1 were inspected via immunochemical technique to demonstrate the anti-metastasis ability of HTPM-gel (Zhang et al., 2023a, 2023b). As depicted in the Fig. 5, the expression of STC-1 was clearly impeded by the HTPM-gel reflect from the decrease of brown areas (black solid arrow). Interestingly, epithelial mesenchymal transition was inhibited by the HTPM-gel, which further indicated the excellent anti-metastasis capability of HTPM-gel (Fig. S6). According to the findings of this study, HTPM-gel successfully suppressed cancer lung metastasis. In addition, BRCA2, a suppressor gene directly linked to hereditary breast cancer, was extensively detected in the CMC recently (Di-Giacomo et al., 2022). Interestingly, HTPM-gel also suppressed the expression of BRCA2, which showed its splendid anticancer activity (Fig. 5). Meanwhile, BRCA2 can also induce the growth of CMC. Therefore, the higher expression of BRCA2 in the Blank-gel augment the proliferation of tumor tissue. As shown in the Fig. S6, HTPM-gel can down-regulate the count of tumor cells to inhibit the growth of CMC. Therefore, we found that mediated cancer therapy and the orthotopic formation of HTPM-gel remarkably inhibited tumors as well as lung metastasis.

3.9. Prognosis efficacy of HTPM-gel on mice with CMC

Tumor cells have a self-protective effect from immune clearance, but surgery does reinforce this immunosuppressive state. The systemic response to wound healing after surgery as well as the resulting inflammation alters immunity. This alteration is characterized by releasing immunosuppressive molecules, such as VEGF and IL-6, transforming growth factor beta (TGF- β), and recruiting immunosuppressive cells, such as M2 macrophages, regulatory T cells (Tregs), and MDSC

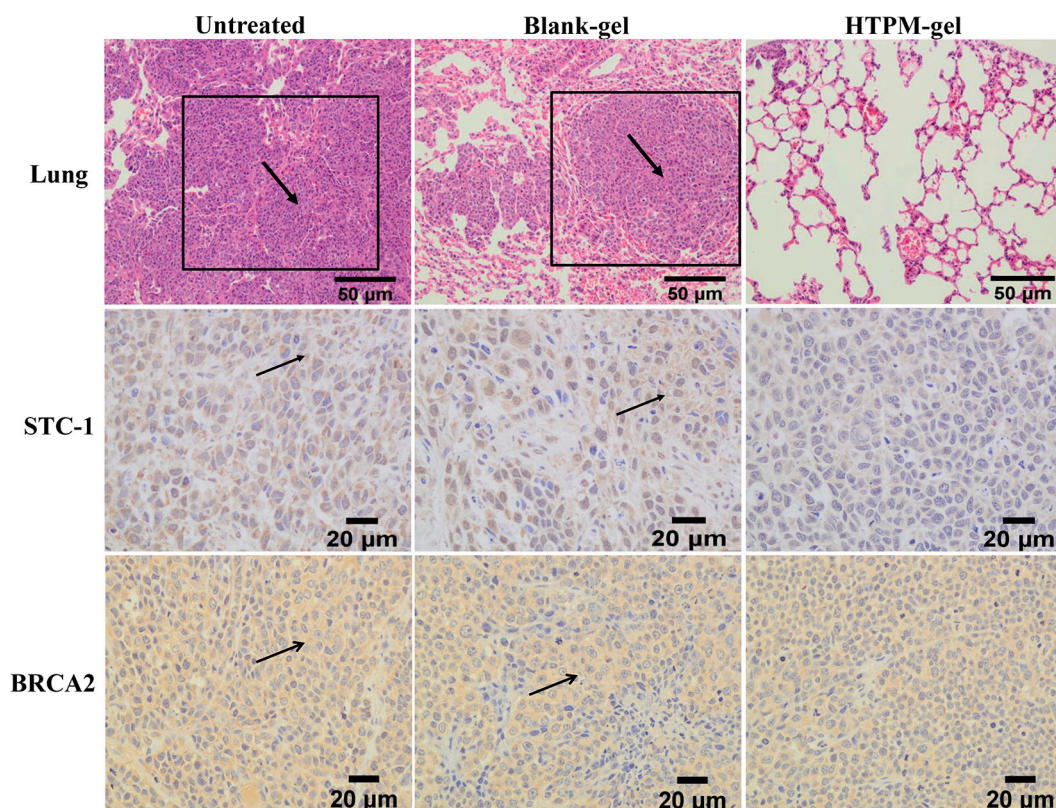


Fig. 5. HTPM-gel suppressed lung metastasis. Histological analysis using H&E staining of lungs from orthotopic tumor-bearing mice treated with the Blank-gel, HTPM-gel (200 \times). The black solid arrow and black box area in the lung slices of the Untreated and Blank-gel groups indicate lungs that appeared to be or were filled with canine mammary carcinoma parenchyma cells. Lung metastasis of tumor tissues from orthotopic CMC tumor-bearing mice treated with the Blank-gel, HTPM-gel. The black-dotted arrow in the analysis of STC-1 and BRCA2 in the Untreated and Blank-gel groups indicate inhibition of lung metastasis of the tumor tissue (400 \times).

(Tang et al., 2020). Prognosis efficacy of postoperative was closely related to proportion of inflammatory cells such as the neutrophil/lymphocyte (NLR) and lymphocyte/monocyte (LMR) ratios. As depicted in the Fig. 6A, B, the NLR and LMR values of the HTPM-gel group were 2.42 ± 0.05 (value <3) and 7.43 ± 0.24 (value >3), respectively, which were correlated with criteria for a good prognosis. Orthotopic injection of the HTPM-gel significantly improved the prognosis of nude mice loaded with CMC. Related study has demonstrated by activating the integrated stress response (IRS), the halofuginone activated the amino acid starvation response (AAR), which selectively inhibited activation of the Th17 cell in mice (Sundrud et al., 2009). As a result, the inflammatory factor secretion from Th17 cells was presumably suppressed and inflammation was reduced because the inflammatory factor secretion decreased (Endo et al., 2021). Th17 cells induce multiple inflammations and exert hematopoietic effects by secreting cytokines such as IL-17A, IL-17F, IL-21, IL-22, and IL-23. As a result, these cytokines have an impact on endothelial cells, epithelial cells, and fibroblasts (Ouyang et al., 2022). For example, IL-17 is a key factor in the recruitment, activation and migration of neutrophils to sites of inflammation (Ye et al., 2001). ELISA reagent kits were used to investigate inflammatory factors, such as IL-17 and IL-22. We found that the HTPM-gel down-regulated IL-17 and IL-22 expression significantly. Thus, HTPM-gel demonstrated its ability to reduce inflammation (Fig. 6C, D). Enhanced extracellular signal-regulated kinase (ERK) signaling, activation of transcription 3 (STAT3), decreased signal transducer, and reduced expression of nuclear factor of activated T cell cytoplasm 1 (NFATC1) are all effects of halofuginone on Th17 cell differentiation (Park et al., 2014).

The tumor microenvironment is closely related to the inflammatory response. The spleen, the largest immune organ in the animal body, contains a multitude of inflammatory cells, such as neutrophils, infiltrating lymphocytes, monocytes, and macrophages. Interestingly, an inflammatory reaction was induced by these inflammatory cells. As depicted in Fig. 6E, neutrophils in the untreated and blank gel groups were significantly increased, whereas lymphocytes were significantly

decreased. Moreover, lymphocytes were slightly enhanced in the HTPM-gel, which indicated that HTPM-gel have an outstanding immunological activity. Previous studies observed increased lymphocyte subsets that depress immunity in diseased dogs under surgical stress. At three days post-surgery, cellular immunosuppression peaked, which could last for two decades (Coffey et al., 2003). Compared with the primary tumors, equal-size recurrent tumors had more immunosuppressive cell infiltration, such as Tregs and M2 macrophages while significantly fewer CD8⁺ T cells. Additionally, within 24 h, pro-tumorigenic cytokines, (e.g., VEGF, IL-1 β , IL-6, IL-10, and TGF- β) increased following surgical resection and IFN- γ , an antitumorigenic cytokine, decreased after surgery (Rosenne et al., 2014). Tumor recurrence is favored in this type of immunosuppressive environment (Predina et al., 2013).

3.10. Effect of HTPM-gel on postoperative site scar formation in CMC bearing mice

In addition to inflammatory cells and inflammatory factors, tumor microenvironment is accompanied by a process of tissue fibrosis (Wu et al., 2023). Furthermore, we found an interesting phenomenon in our experiments reflected from the post-operative wound sutures in the HTPM-gel-treated group of nude rats exhibited well healed and no scars were present. As shown in the Fig. 7A, the model diagram clearly depicts the efficacy of HTPM-gel on postoperative CMC bearing nude mice. Importantly, the post-operative suture sites of nude mice in the recovery period were observed no scar with perfect healing. Previous studies indicated the halofuginone inhibited the proliferation of keloid fibroblasts in a sustained manner, limiting the migration of keloid fibroblasts over time and inhibiting TGF- β -induced myofibroblast transformation and ECM re-modelling (Popov et al., 2006). Meanwhile, halofuginone, as an inhibitor of Collagen I and promoter of TGF- β , can efficiently improve post-operative wound healing manifested in the inhibition of expression for Collagen I and enhancement for TGF- β , which indicated in the Fig. 7B. Critical inflammatory cytokines, including TNF- α and IL-6, are important in the process of healing wounds (Leiba et al., 2006). It

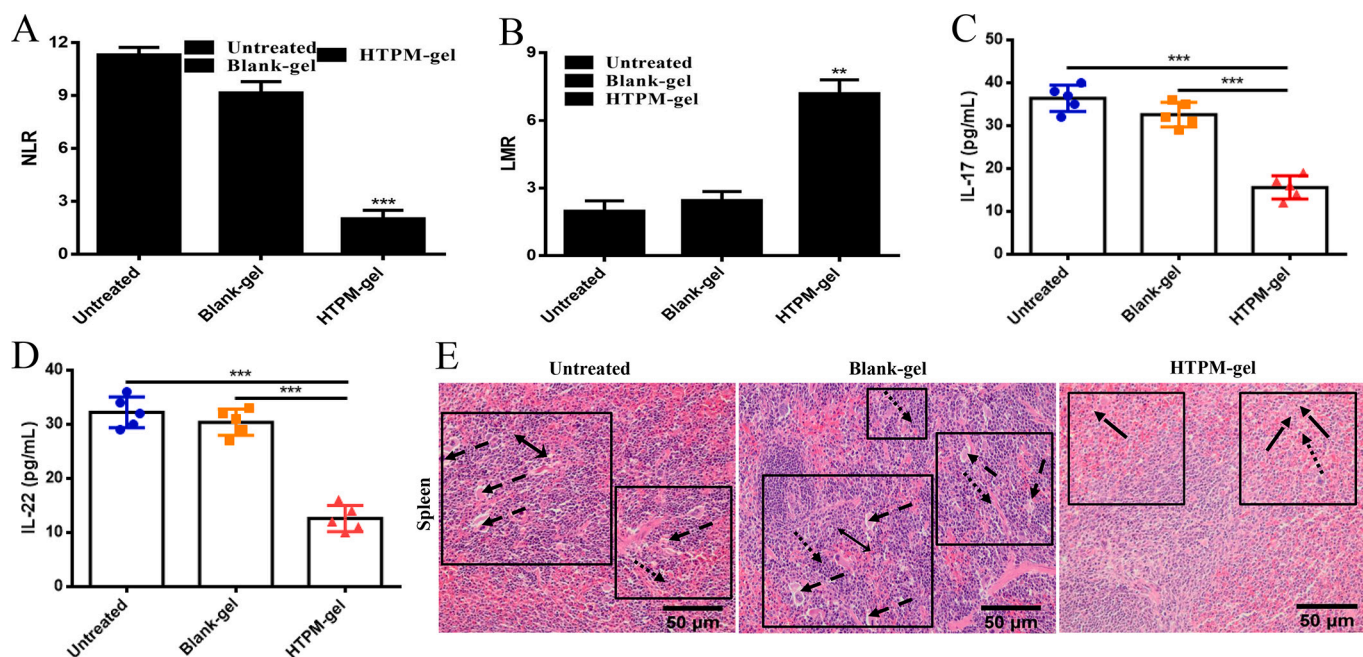


Fig. 6. Prognosis of mice with orthotopic tumors treated with the Blank-gel, HTPM-gel. (A) NLR and (B) LMR (NLR: neutrophil granulocyte/lymphocyte ratio, LMR: lymphocyte/monocyte ratio) of nude mice after administration of Untreated, Blank gel, HTPM-gel ($n = 5$). (C&D) We used an ELISA reagent kit to detect the representative inflammatory factors secreted by Th cells, such as IL-22 and IL-17, from the serum ($n = 5$). (E) Histological analysis of spleens from mice with orthotopic tumors treated with the Blank-gel, HTPM-gel using H&E staining (200 \times). The black open arrows, black solid arrows, black dotted arrows, and black square-pointed arrows in the spleen images represent the neutrophils, infiltrating lymphocytes, monocytes, and macrophages, respectively, of the Untreated and Blank-gel groups.

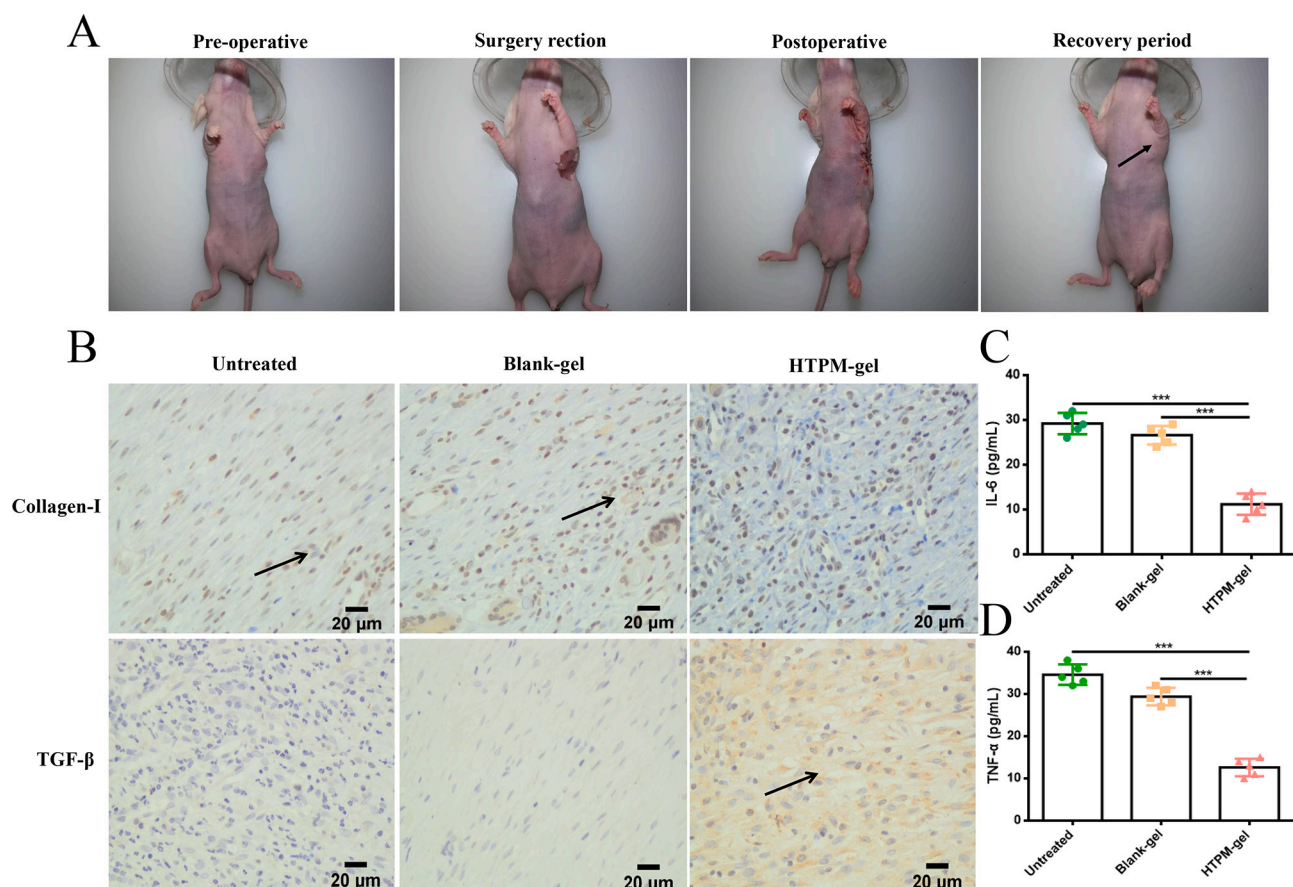


Fig. 7. Effect of HTPM-gel on the scar from the postoperative site. (A) Representative images indicated the excellent scar removal capability of HTPM-gel which was shown in the recovery period of CMC bearing mice. (B) Collagen I and TGF- β , as key factors in scar formation, were investigated via immunohistochemical technique (400 \times). Black dovetail arrow in the Collagen I image of the Untreated and Blank gel group indicate scar formation of the skin tissue. Black open arrow in the TGF- β images of the HTPM-gel indicates healing degree of the skin tissue. (C&D) We used an ELISA reagent kit to detect representative inflammatory factors, such as IL-6 and TNF- α , from the serum (n = 5).

is noteworthy that IL-6 and TNF- α were significantly suppressed by halofuginone released from the HTPM-gel (Fig. 7C, D). This result was further demonstrated by the immunohistochemical analysis in the Fig. S8. The ECM produced by myfibroblasts after the activation of halofuginone acts as microenvironment for the survival of breast tissue and has a role in maintaining the continuity and integrity of the breast tissue acted as an adipose tissue. Keloids are characterized by increased deposition of fibrous tissue in the subcutaneous tissue (adipose tissue) following an abnormal wound healing process. Myfibroblasts play a large role in the wound healing and keloids (Marty et al., 2021). More importantly, halofuginone can inhibit the formation of scar via impeding the expression of TGF- β and Smad-3 in TGF- β &Smad-3 pathway and attenuate Collagen synthesis with exerting anti-fibrotic action mechanisms (Marty et al., 2021). Above results support therapeutic use of HTPM-gel for scar removal and postoperative breast tissue wound healing.

3.11. Safety of HTPM-gel in CMC-bearing mice

Every two days during the whole animal experiment, we monitored the body weights and found that body weights in all the mice groups increased over time. Obvious body weight changes were not observed among the groups (Fig. 4B). Halofuginone leads to toxicity by inducing apoptosis; however, HTPM or HTPM-gel decreased halofuginone toxicity. To predict the injury of main organs in nude mice, hematological indicators were tested such as HGB and PLT, and biochemistry parameters, such as alanine aminotransferase (ALT) and

aminotransferase (AST) (Pinheiro et al., 2019). Compared with the Blank-gel, the physiological index such as HGB of the SD rats treated with HTPM-gel showed no obvious changes (Fig. 8B). Notably, the expression level of PLT was significantly increased in the HTPM-gel compared with Blank-gel (Fig. 8C). The levels of AST and ALT did not change significantly in HTPM-gel-treated mice (Fig. 8D–E), which showed that HTPM-gel have potential biocompatibility. The results collectively suggest that the HTPM&AgNPs-gel display good biocompatibility and are safety for tissue engineering applications. HTPM-gel did not lead to significant differences in the hematological indexes relative to Untreated and Blank-gel group. In HTPM-gel-treated mice, we did not observe any clear pathological changes in the liver, heart, or other organs. Thus, the HTPM-gel was determined to be reliably safe (Fig. 8A). As we had assumed, an overdose of halofuginone induced toxicity, whereas the encapsulated halofuginone in TPGS polymer micelles were passively targeted to tumor tissues and prepared into HTPM-gel. In preclinical studies, this led to CMC growth and metastasis being strongly suppressed, as well as satisfactory safety.

4. Discussion

According to the criteria for determining the properties of temperature-sensitive gels, the gelling temperature should be higher than room temperature and lower than with closing to the body temperature of the test subject (the test subject in this experiment is a dog, so the appropriate gelling temperature is 37.5 $^{\circ}$ C ~ 38.5 $^{\circ}$ C), and the optimal gelling time was acquired when its value was shorter. As

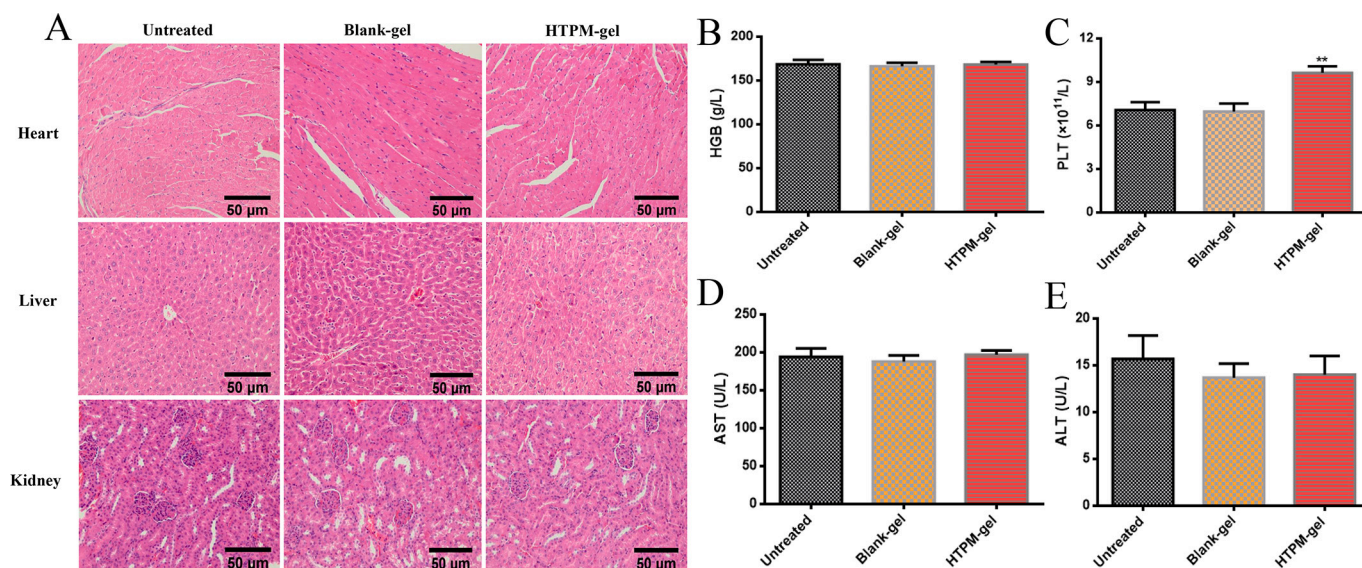


Fig. 8. Safety evaluation of biocompatibility of orthotopic CMC-bearing mice treated with the Blank-gel, HTPM-gel. (A) Representative images of primary organs such as heart, liver and kidney in mice from H&E staining (200 \times), $n = 5$. (B&C) Representative blood physiology indicators such as hemoglobin (HGB) and platelet (PLT) in the serum of mice were determined, $n = 5$. (D&E) We determined alanine transaminase (ALT) and serum aspartate transaminase (AST) as the representative blood biochemical indicators of mice ($n = 5$).

depicted in the Table S1 and Table S2, it can be seen that when the formulation ratio of poloxamer 407 and poloxamer 188 is 9 g: 2 g, the gelation temperature is within the appropriate temperature range and the gelation time is shorter, so above proportion is determined to be the final formulation. Furthermore, when the stirring speed was 100 rpm, gel temperature (37.6 ± 0.2 °C) and gel time (89.6 ± 0.5 s) of poloxamer thermos-sensitive gel was both in the optimal state compared with other two stirring speed (Table S3). HTPM-gel, as a novel development localized postoperative therapy, have numerous excellent characterizations. HTPM-gel were positively charged, with a ZP of 15.10 ± 1.82 mV (Fig. S2B). The mutual repulsion between particles was better and the system was stable (Augustine et al., 2020). The Because of electrostatic interactions, positively charged HTPM interacted with negatively charged intestinal mucouscan prolong intestinal retention time (Wang et al., 2019). More importantly, the mechanism by which the HTPM-gel exhibiting thermos-sensitivity was mainly rely on poloxamer thermos-sensitive gel. Poloxamer is a non-ionic surfactant, which has a special spherical micelle structure in aqueous solution, with hydrophobic polypropylene oxide (PPO) as the core and hydrophilic polyethylene oxide (PEO) as the shell. When the ambient temperature is higher than the critical micellar temperature, and meanwhile the concentration of poloxamer reaches the critical micellar concentration, the water molecules on the hydrophobic segments will be continuously detached and further forming micelles. Moreover, when the temperature is further increased, the water molecules on the hydrophilic segments will be detached as well, and they will be entangled with each other. Interestingly, when the concentration of the micelles reaches the critical volume fraction, the micelles piled up closely and formed a semi-solid gel (Liu et al., 2024). Therefore, poloxamer is a free-flowing liquid at low temperatures and a semi-solid gel at high temperatures. In addition, poloxamer 407, a copolymer of poly (oxyethylene)-poly (oxypropylene)-poly (oxyethylene), is a well-known thermo-sensitive matrix and can exhibit reversible solution (sol)–gelation (gel) transition in an aqueous solution. With good temperature sensitivity, poloxamer 407 is an ideal excipient to prepare temperature-sensitive in situ gel acting as a depot for controlled release of drugs via convenient local administration (Gao et al., 2016). More importantly, inspired by the hydrogels made from other amphiphilic molecules, thermosensitive TPGS hydrogels were firstly discovered and developed in the presence of specific anions, which self-assembled from the aggregation of TPGS micelles stimulated

by heating and salting-out effect (Xiong et al., 2023).

Because of the hydrogen bond between the water and hydrophilic molecules, when the temperature was below 37 °C (less than LCST) of gel, the hydrogel with the hydration layer of the hydrophobic group had better water absorption properties. When the temperature was higher than the LCST, the interaction of hydrophobic groups was pivotal. As the gel volume shrank, the polymer chain shrank and aggregated (Dehghan-Baniani et al., 2017). Meanwhile, the swelling rate of the hydrogel eventually tends to a certain value due to the influence of factors such as the inhibition of other ions in the water, further the swelling effect of the hydrogel disappeared, therefore the swelling rate does not change no more (Potta et al., 2009). The swelling mechanism of hydrogels involves numerous factors, including the molecular structure of the polymer, crosslink density, intermolecular interactions, and ionic strength in solution. The molecular structure of the polymer has a significant effect on the swelling properties of hydrogels (Truong et al., 2017). The higher the molecular weight and molecular weight distribution of the polymer, the weaker the interaction force between its molecular chains, which leads to the higher swelling performance of the hydrogel. When the molecular weight reaches a certain level, the network structure becomes looser and therefore can accommodate more water molecules. The crosslink density of the polymer is also a critical factor in the swelling properties of hydrogels (Lee et al., 2019). The higher the interconnection density, the tighter the network structure of the hydrogel, thus making it more difficult to adsorb water molecules. Conversely, a low-density crosslinked structure will make it easier for the hydrogel to absorb water molecules. As mention above, the length and relative proportion of PEO and PPO chain segments in the molecule of polymer affect the swelling behavior of the hydrogel, and the effect of PPO is dominant (Galocha-León et al., 2023). The number and relative proportion of PO in the molecule of polymer 407 (EO100PO85EO100) is higher than that of polymer 188 (EO76PO29EO76), while the relative proportion of EO is lower. Alternatively, poloxamer can bind TPGS to form a cross-linked network thereby influencing the swelling behavior of the hydrogel to a certain extent (Gao et al., 2016). Additionally, HTPM-gel (needle: 29 G) exhibit more excellent injectability compared with other hydrogels especially poloxamer hydrogels (needle: 21 G), which reflected the convenience and speed in injection (Yang et al., 2018). Interestingly, the number in front of G was the larger, the needle was the thinner with the easier and quicker injectability.

DSC and TG were used to investigate the thermal stability and decomposition behavior of HTPM-gel. Remarkably, HTPM-gel can remove the scar in the postoperative mice with good capabilities owing to the release of halofuginone, compared with other current commercially available chemotherapy drugs and gel products. More importantly, HTPM-gel also have splendid biocompatibility as shown in the Fig. 8. Combining the above descriptions, HTPM-gel have magnanimous advantages as a potential local chemotherapeutic agent and pro-wound healing drugs in the postoperative CMC and human triple-negative cancer. Angiogenesis is necessary for tumor progression so that the tumor cells can escape into the bloodstream and establish metastatic colonies in secondary sites (Loges et al., 2009). Tumor lymph-angiogenesis is essential to disseminate lymphatic metastases (Bielenberg and Zetter, 2015). Quantitative micro-vessel density (MVD) counting is one of the most important tools for studying angiogenesis in tumor tissues (Zhang et al., 2022). MVD analysis methods can assess the angiogenic capacity of tumors by quantitatively measuring the number of neovessels in tumor tissues and provide an important basis for tumor micro-vessel localization therapy and prognostic assessment. Herein, immunohistochemical staining is a commonly used method for MVD analysis (Rossi et al., 2010). This method distinguishes blood vessels from surrounding tissues by labelling them with vascular endothelial cell-specific antigens (e.g. CD31, etc.) and thus counts the number of blood vessels. Meanwhile, the molecular biomarker approach of MVD is analyzed by detecting relevant angiogenic markers (e.g. VEGF, etc.) (Bennani-Baiti et al., 2020). Thus, the number of vessels and sizes can be obtained from Figs. S6-S7. Tumor metastasis is a significant malignant feature of CMC and causes >90% of deaths related to CMC (Li et al., 2023). Further, lung metastasis related pivotal protein STC-1 were inspected via immunochemical technique to demonstrate the anti-metastasis ability of HTPM-gel (Zhang et al., 2023a, 2023b). Meanwhile, BRCA2, a suppressor gene directly linked to hereditary breast cancer, was extensively detected in the CMC recently (Di-Giacomo et al., 2022). As shown in the Fig. 5, the expression of STC-1 and BRCA2 were significantly impeded by HTPM-gel compared with Blank-gel, which indicated HTPM-gel can inhibit the tumor metastasis. The tumor microenvironment (TME) has substantial inflammatory factors, including IL-6, IL-17, IL-22, and TNF- α (Lian et al., 2023). Tumor progression and initiation of tumors are complex and they do not exist in isolation from the organism. Thus, the tumor's microenvironment is intimately tied to tumor growth, motility, proliferation, and immunosuppressive response. According to the cancer evolution-development hypothesis, the synergistic effect of immune genetic factors causes the dysregulation of immune balance. Additionally, environmental factors maintain and stimulate inflammation that does not resolve. This inflammation creates a microenvironment throughout the cancer development process, causing cancer to evolve and develop (Zhao et al., 2023). Further, the presence of these inflammatory factors can induce the development of an inflammatory response thereby further increasing tumor metastasis and recurrence. Another factor contributing to tumor recurrence is the plasticity of non-stem-cancer cells and the acquisition of cancer stem cell (CSC) functionality (Ritter et al., 2023). The identity of CMC cell line CMT-U27 was examined and found CSCs in many solid tumors. These CSC are pivotal in tumor recurrence, occurrence, and metastasis (Yao et al., 2023). Because of their limited number and location in oxygen-deprived tissue far from the blood vessels, it is difficult for drugs to kill CSCs (Molfetta et al., 2023). The survival and stemness maintenance of CSCs depends on the TME. Future studies will investigate the mechanisms and effect of HTPM-gel on human breast and canine mammary CSCs. Moreover, we aspire to develop HTPM-gel as a novel postoperative therapeutic agent for canine mammary carcinoma and human triple-negative breast cancer.

5. Conclusions

In this study, we achieved simultaneous ablation of tumor growth

and metastasis with scar removal. Using this novel chemotherapy strategy, a natural small molecule self-assembled hydrogel of HTPM was designed following a one-step approach. This HTPM-gel significantly suppressed tumor growth and inhibited lung metastasis. We did not observe toxicity at a dose of 0.25 mg/kg and achieved an inhibition rate of tumor growth >75%. We also assessed the ability of HTPM-gel to inhibit tumor growth and prevent lung metastasis through its antitumor mechanism and decreased inflammatory reaction. Furthermore, HTPM-gel can effectively remove the scar in the post-operative wound site. According to results of this study, the amount of HTPM-gel is useful as a biomarker for diagnosis, monitoring, and prognosis of CMC. Thus, we confirmed that HTPM-gel is a promising biocompatible nanomedicine to treat postoperative metastatic and angiogenic CMC. This niche-like hydrogel is promising for further clinical translation and holds major implications for antitumor therapy.

CRedit authorship contribution statement

Runan Zuo: Writing – review & editing, Writing – original draft, Visualization, Validation, Project administration, Methodology, Investigation, Funding acquisition, Formal analysis, Conceptualization. **Lingqing Kong:** Writing – review & editing, Validation, Investigation. **Wanjun Pang:** Writing – review & editing, Validation, Investigation. **Shanxiang Jiang:** Writing – review & editing, Validation, Supervision, Resources, Formal analysis, Conceptualization.

Declaration of competing interest

The authors declare that they have no known competing financial interests or personal relationships that could have appeared to influence the work reported in this paper.

Data availability

Data will be made available on request.

Acknowledgements

This work was supported by the grants from the Key Projects of Natural Science Foundation of Anhui Provincial Department of Education (2023AH051017) and the Anhui Agricultural University Talent Research Grant Project (rc393302). We thank Let-Pub (www.letpub.com) for its linguistic assistance during the preparation of this manuscript.

Appendix A. Supplementary data

Supplementary data to this article can be found online at <https://doi.org/10.1016/j.ijpx.2024.100241>.

References

- Agrawal, M., Saraf, S., Saraf, S., Dubey, S.K., Puri, A., Gupta, U., Kesharwani, P., Ravichandiran, V., Kumar, P., Naidu, V.G.M., Murty, U.S., Ajazuddin, Alexander A., 2020. Stimuli-responsive in situ gelling system for nose-to-brain drug delivery. *J. Control. Release* 327, 235–265.
- Ali, I., Rizwan, A., Vu, T.T., Jo, S.H., Oh, C.W., Kim, Y.H., Park, S.H., Lim, K.T., 2024. NIR-responsive carboxymethyl-cellulose hydrogels containing thioketal-linkages for on-demand drug delivery system. *Int. J. Biol. Macromol.* 260 (Pt 2), 129549.
- Alonso-Miguel, D., Valdivia, G., García-San-José, P., Alonso-Diez, Á., Clares, I., Portero, M., Peña, L., Pérez-Alenza, M.D., 2022. Clinical outcome of dogs diagnosed with canine inflammatory mammary cancer treated with metronomic cyclophosphamide, a cyclooxygenase-2 inhibitor and toceranib phosphate. *Vet. Comp. Oncol.* 20 (1), 179–188.
- Altuntaş, E., Yener, G., 2017. Formulation and evaluation of thermoreversible in situ nasal gels containing mometasone furoate for allergic rhinitis. *AAPS Pharm. Sci. Tech.* 18 (7), 2673–2682.
- Augustine, R., Kim, D.K., Kalva, N., Eom, K.H., Kim, J.H., Kim, I., 2020. Multi-stimuli-responsive nanomicelles fabricated using synthetic polymer polylysine conjugates

- for tumor microenvironment dependent drug delivery. *J. Mater. Chem. B* 8 (26), 5745–5755.
- Bennani-Baiti, B., Pinker, K., Zimmermann, M., Helbich, T.H., Baltzer, P.A., Clauser, P., Kapetas, P., Bago-Horvath, Z., Stadlbauer, A., 2020. Non-invasive assessment of hypoxia and neovascularization with MRI for identification of aggressive breast cancer. *Cancers (Basel)* 12 (8), 2024.
- Bielenberg, D.R., Zetter, B.R., 2015. The contribution of angiogenesis to the process of metastasis. *Cancer J.* 21 (4), 267–273.
- Boix-Montesinos, P., Soriano-Teruel, P.M., Armiñán, A., Orzáez, M., Vicent, M.J., 2021. The past, present, and future of breast cancer models for nanomedicine development. *Adv. Drug Deliv. Rev.* 173, 306–330.
- Chen, Q., Wang, C., Zhang, X., Chen, G., Hu, Q., Li, H., Wang, J., Wen, D., Zhang, Y., Lu, Y., Yang, G., Jiang, C., Wang, J., Dotti, G., Gu, Z., 2019. In situ sprayed bioresponsive immunotherapeutic gel for post-surgical cancer treatment. *Nat. Nanotechnol.* 14 (1), 89–97.
- Chen, A., Ye, S., Zheng, J., Li, J., Chen, Z., Zhang, Y., Li, S., 2023. Establishment and characterization of a Her2-enriched canine mammary cancerous myoepithelial cell line. *BMC Vet. Res.* 19 (1), 22.
- Coffey, J., Wang, J., Smith, M., Bouchier-Hayes, D., Cotter, T., Redmond, H., 2003. Excisional surgery for cancer cure: therapy at a cost. *Lancet Oncol.* 4 (12), 760–768.
- de Jonge, M.J., Dumez, H., Verweij, J., Yarkoni, S., Snyder, D., Lacombe, D., Marréaud, S., Yamaguchi, T., Punt, C.J., van Oosterom, A., 2006. Phase I and pharmacokinetic study of halofuginone, an oral quinazolinone derivative in patients with advanced solid tumours. *Eur. J. Cancer* 42, 1768–1774.
- de Oliveira, J.T., Santos, A.L., Gomes, C., Barros, R., Ribeiro, C., Mendes, N., de Matos, A. J., Vasconcelos, M.H., Oliveira, M.J., Reis, C.A., Gärtner, F., 2015. Anti-influenza neuraminidase inhibitor oseltamivir phosphate induces canine mammary cancer cell aggressiveness. *PLoS One* 10 (4) e0121590.
- De, L.I., Di, C.F., Conte, R., Peluso, G., Cerruti, P., Calarco, A., 2023. In-Situ thermoresponsive hydrogel containing resveratrol-loaded nanoparticles as a localized drug delivery platform for dry eye disease. *Antioxidants (Basel)* 12 (5), 993.
- Dehghan-Baniani, D., Bagheri, R., Solouk, A., 2017. Preparation and characterization of a composite biomaterial including starch micro/nano particles loaded chitosan gel. *Carbohydr. Polym.* 174, 633–645.
- Deng, X., Lin, D., Zhang, X., Shen, X., Yang, Z., Yang, L., Lu, X., Yu, L., Zhang, N., Lin, J., 2020. Profiles of immune-related genes and immune cell infiltration in the tumor microenvironment of diffuse lower-grade gliomas. *J. Cell. Physiol.* 235 (10), 7321–7331.
- Dethe, M.R., Ahmed, H., Agrawal, M., Roy, U., Alexander, A., 2022. PCL-PEG copolymer based injectable thermosensitive hydrogels. *J. Control. Release* 343, 217–236.
- Di-Giacomo, D., Di-Domenico, M., Defourny, S.V.P., Malatesta, D., Di-Teodoro, G., Martino, M., Viola, A., D’Alterio, N., Cammà, C., Modesto, P., Pettrini, A., 2022. Validation of AmpliSeq NGS Panel for BRCA1 and BRCA2 variant detection in canine formalin-fixed paraffin-embedded mammary tumors. *Life (Basel)* 12 (6), 851.
- Endo, K., Matsui, R., Asami, T., Sawa, T., Nakashima, A., Tanaka, Y., Makabe, H., Tanaka, S., 2021. The suppression of IL-17 production from T cells by gallate-type procyanidin is mediated by selectively inhibiting cytokine production from dendritic cells. *Biomed. Pharmacother.* 137, 111346.
- Galocha-León, C., Antich, C., Voltres-Martínez, A., Marchal, J.A., Mallandrich, M., Halbaut, L., Rodríguez-Lagunas, M.J., Souto, E.B., Clares-Naveros, B., Gálvez-Martín, P., 2023. Development and characterization of a poloxamer hydrogel composed of human mesenchymal stromal cells (hMSCs) for reepithelization of skin injuries. *Int. J. Pharm.* 647, 123535.
- Gao, L., Wang, X., Ma, J., Hao, D., Wei, P., Zhou, L., Liu, G., 2016. Evaluation of TPGS-modified thermo-sensitive Pluronic PF127 hydrogel as a potential carrier to reverse the resistance of P-gp-overexpressing SMMC-7721 cell lines. *Colloids Surf. B: Biointerfaces* 140, 307–316.
- Hammad, R.W., Sanad, R.A., Abdelmalak, N.S., Torad, F.A., Latif, R., 2020. New intranasal cross-linked mosapride xyloglucan pluronic micelles (MOS-XPMS) for reflux esophagitis disease: in-vitro optimization and improved therapeutic efficacy. *J. Adv. Res.* 23, 83–94.
- Hou, M., Wang, X., Yue, O., Zheng, M., Zhang, H., Liu, X., 2022. Development of a multifunctional injectable temperature-sensitive gelatin-based adhesive double-network hydrogel. *Biomater. Adv.* 134, 112556.
- Lan, L.H., Sun, B.B., Zuo, B.X., Chen, X.Q., Du, A.F., 2017. Prevalence and drug resistance of avian *Eimeria* species in broiler chicken farms of Zhejiang province, China. *Poult. Sci.* 96 (7), 2104–2109.
- Lavalle, G.E., De-Campos, C.B., Bertagnoli, A.C., Cassali, G.D., 2012. Canine malignant mammary gland neoplasms with advanced clinical staging treated with carboplatin and cyclooxygenase inhibitors. *In Vivo* 26 (3), 375–379.
- Lee, Y.P., Liu, H.Y., Lin, P.C., Lee, Y.H., Yu, L.R., Hsieh, C.C., Shih, P.J., Shih, W.P., Wang, L.J., Yen, J.Y., Dai, C.A., 2019. Facile fabrication of superporous and biocompatible hydrogel scaffolds for artificial corneal periphery. *Colloids Surf. B: Biointerfaces* 175, 26–35.
- Lee, S.Y., Jeon, S.I., Sim, S.B., Byun, Y., Ahn, C.H., 2021. A supramolecular host-guest interaction-mediated injectable hydrogel system with enhanced stability and sustained protein release. *Acta Biomater.* 131, 286–301.
- Leiba, M., Cahalon, L., Shimoni, A., Lider, O., Zanin-Zhorov, A., Hecht, I., Sela, U., Vlodavsky, I., Nagler, A., 2006. Halofuginone inhibits NF-kappaB and p38 MAPK in activated T cells. *J. Leukoc. Biol.* 80 (2), 399–406.
- Li, X., Lin, Z., Wang, P., Zhou, C., Xu, J., Lin, J., Lin, D., Zhang, D., 2023. Tetramethylpyrazine-Rhein Derivative inhibits the migration of canine inflammatory mammary carcinoma cells by mitochondrial damage-mediated apoptosis and cadherins downregulation. *Biomed. Pharmacother.* 162, 114731.
- Lian, J., Lin, D., Huang, Y., Chen, X., Chen, L., Zhang, F., Tang, P., Xie, J., Hou, X., Du, Z., Deng, J., Hao, E., Liu, J., 2023. Exploring the potential use of Chinese herbs in regulating the inflammatory microenvironment of tumours based on the concept of ‘state-target identification and treatment’: a scoping review. *Chin. Med.* 18 (1), 124.
- Liu, Y., Ma, W., Zhou, P., Wen, Q., Wen, Q., Lu, Y., Zhao, L., Shi, H., Dai, J., Li, J., Fu, S., 2023. In situ administration of temperature-sensitive hydrogel composite loading paclitaxel microspheres and cisplatin for the treatment of melanoma. *Biomed. Pharmacother.* 160, 114380.
- Liu, X., Ding, Q., Liu, W., Zhang, S., Wang, N., Chai, G., Wang, Y., Sun, S., Zheng, R., Zhao, Y., Ding, C., 2024. A Poloxamer 407/chitosan-based thermosensitive hydrogel dressing for diabetic wound healing via oxygen production and dihydromyricetin release. *Int. J. Biol. Macromol.* 263 (Pt 1), 130256.
- Loges, S., Mazzone, M., Hohensinner, P., Carmeliet, P., 2009. Silencing or fueling metastasis with VEGF inhibitors: antiangiogenesis revisited. *Cancer Cell* 15 (3), 167–170.
- Marty, P., Chatelain, B., Lihoreau, T., Tissot, M., Dirand, Z., Humbert, P., Senez, C., Secomandi, E., Isidoro, C., Rolin, G., 2021. Halofuginone regulates keloid fibroblast fibrotic response to TGF-β induction. *Biomed. Pharmacother.* 135, 111182.
- Michishita, M., Ochiai, K., Nakahira, R., Azakami, D., Machida, Y., Nagashima, T., Nakagawa, T., Ishiwata, T., 2023. mTOR pathway as a potential therapeutic target for cancer stem cells in canine mammary carcinoma. *Front. Oncol.* 13, 1100602.
- Molfetta, R., Lecce, M., Milito, N.D., Putro, E., Pietropaolo, G., Marangio, C., Scarno, G., Moretti, M., De, Smaele E., Santini, T., Bernardini, G., Sciumè, G., Santoni, A., Paolini, R., 2023. SCF and IL-33 regulate mouse mast cell phenotypic and functional plasticity supporting a pro-inflammatory microenvironment. *Cell Death Dis.* 14 (9), 616.
- Ouyang, K., Oparaugo, N., Nelson, A.M., Agak, G.W., 2022. T cell extracellular traps: tipping the balance between skin health and disease. *Front. Immunol.* 13, 900634.
- Park, M.K., Park, J.S., Park, E.M., Lim, M.A., Kim, S.M., Lee, D.G., Baek, S.Y., Yang, E.J., Woo, J.W., Lee, J., Kwok, S.K., Kim, H.Y., Cho, M.L., Park, S.H., 2014. Halofuginone ameliorates autoimmune arthritis in mice by regulating the balance between Th17 and Treg cells and inhibiting osteoclastogenesis. *Arthritis Rheum.* 66 (5), 1195–1207.
- Pinheiro, W.O., Fascinel, M.L., Farias, G.R., Horst, F.H., de Andrade, L.R., Corrêa, L.H., Magalhães, K.G., Sousa, M.H., de Almeida, M.C., Azevedo, R.B., Lacava, Z.G.M., 2019. The influence of female mice age on biodistribution and biocompatibility of citrate-coated magnetic nanoparticles. *Int. J. Nanomedicine* 14, 3375–3388.
- Poirier, V.J., Hershey, A.E., Burgess, K.E., Phillips, B., Turek, M.M., Forrest, L.J., Beaver, L., Vail, D.M., 2004. Efficacy and toxicity of paclitaxel (Taxol) for the treatment of canine malignant tumors. *J. Vet. Intern. Med.* 18 (2), 219–222.
- Popov, Y., Patscher, E., Bauer, M., Niedobitek, E., Schulze-Krebs, A., Schuppan, D., 2006. Halofuginone induces matrix metalloproteinases in rat hepatic stellate cells via activation of p38 and NFκappaB. *J. Biol. Chem.* 281 (22), 15090–15098.
- Potta, T., Chun, C., Song, S.C., 2009. Chemically crosslinkable thermosensitive polyphosphazene gels as injectable materials for biomedical applications. *Biomaterials.* 30 (31), 6178–6192.
- Predina, J., Eruslanov, E., Judy, B., Kapoor, V., Cheng, G., Wang, L.C., Sun, J., Moon, E. K., Fridlender, Z.G., Albelda, S., Singhal, S., 2013. Changes in the local tumor microenvironment in recurrent cancers may explain the failure of vaccines after surgery. *Proc. Natl. Acad. Sci. U. S. A.* 110 (5), E415–E424.
- Ritter, A., Kreis, N.N., Roth, S., Friemel, A., Safdar, B.K., Hoock, S.C., Wildner, J.M., Allert, R., Louwen, F., Solbach, C., Yuan, J., 2023. Cancer-educated mammary adipose tissue-derived stromal/stem cells in obesity and breast cancer: spatial regulation and function. *J. Exp. Clin. Cancer Res.* 42 (1), 35.
- Rocha, M.S., Batista, J.V.C., Melo, M.N.O., Campos, V.E.B., Toledo, A.L.M.M., Oliveira, A.P., Picciani, P.H.S., Baumgartner, S., Holandino, C., 2022. Pluronic® F127 Thermoresponsive viscum album hydrogel: physicochemical features and cellular in vitro evaluation. *Pharmaceutics.* 14 (12), 2775.
- Rosenne, E., Sorski, L., Shaashua, L., Neeman, E., Matzner, P., Levi, B., Ben-Eliyahu, S., 2014. In vivo suppression of NK cell cytotoxicity by stress and surgery: glucocorticoids have a minor role compared to catecholamines and prostaglandins. *Brain Behav. Immun.* 37, 207–219.
- Rossi, B., Schinzari, G., Maccauro, G., Scaramuzza, L., Signorelli, D., Rosa, M.A., Fabbriani, C., Carlo, B., 2010. Neoadjuvant multidrug chemotherapy including high-dose methotrexate modifies VEGF expression in osteosarcoma: an immunohistochemical analysis. *BMC Musculoskelet. Disord.* 11, 34.
- Santos, D.B., Fernandez, G.J., Pardini, L.M.C., Pardini, M.I.M.C., Ferrasi, A.C., 2023. Transcriptomic profile of canine mammary ductal carcinoma. *Int. J. Mol. Sci.* 24 (6), 5212.
- Sassi, A., Kacem, B., Hassairi, A., Jaidane, M., Saguem, S., 2018. Formulation and evaluation of topical halofuginone gel using a novel ex vivo model. *Trop. J. Pharm. Res.* 17 (5), 755–760.
- Simon, D., Schoenrock, D., Baumgärtner, W., Nolte, I., 2006. Postoperative adjuvant treatment of invasive malignant mammary gland tumors in dogs with doxorubicin and docetaxel. *J. Vet. Intern. Med.* 20 (5), 1184–1190.
- Sundrud, M.S., Koralov, S.B., Feuerer, M., Calado, D.P., Kozhaya, A.E., Rhule-Smith, A., Lefebvre, R.E., Unutmaz, D., Mazitschek, R., Waldner, H., Whitman, M., Keller, T., Rao, A., 2009. Halofuginone inhibits TH17 cell differentiation by activating the amino acid starvation response. *Science.* 324 (5932), 1334–1338.
- Tan, Y., Sun, R., Liu, L., Yang, D., Xiang, Q., Li, L., Tang, J., Qiu, Z., Peng, W., Wang, Y., Ye, L., Ren, G., Xiang, T., 2021. Tumor suppressor DRD2 facilitates M1 macrophages and restricts NF-κB signaling to trigger pyroptosis in breast cancer. *Theranostics.* 11 (11), 5214–5231.

- Tang, F., Tie, Y., Tu, C., Wei, X., 2020. Surgical trauma-induced immunosuppression in cancer: recent advances and the potential therapies. *Clin. Transl. Med.* 10 (1), 199–223.
- Torres-Figueroa, A.V., Pérez-Martínez, C.J., Encinas, J.C., Burruel-Ibarra, S., Silvas-García, M.I., García-Alegria, A.M., Del-Castillo-Castro, T., 2021. Thermosensitive bioadhesive hydrogels based on poly(N-isopropylacrilamide) and poly(methyl vinyl ether-alt-maleic anhydride) for the controlled release of metronidazole in the vaginal environment. *Pharmaceutics*. 13 (8), 1284.
- Touzout, Z., Abdellaoui, N., Hadj-Hamou, A.S., 2024. Conception of pH-sensitive calcium alginate/poly vinyl alcohol hydrogel beads for controlled oral curcumin delivery systems. Antibacterial and antioxidant properties. *Int. J. Biol. Macromol.* 263, 130389.
- Truong, V.X., Tsang, K.M., Forsythe, J.S., 2017. Nonswelling click-cross-linked gelatin and PEG hydrogels with tunable properties using pluronic linkers. *Biomacromolecules*. 18 (3), 757–766.
- Urner, S., Planas-Paz, L., Hilger, L.S., Henning, C., Branopolski, A., Kelly-Goss, M., Stanczuk, L., Pitter, B., Montanez, E., Peirce, S.M., Mäkinen, T., Lammert, E., 2019. Identification of ILK as a critical regulator of VEGFR3 signalling and lymphatic vascular growth. *EMBO J.* 38 (2), e99322.
- Valdivia, G., Alonso-Diez, Á., Pérez-Alenza, D., Peña, L., 2021. From conventional to precision therapy in canine mammary cancer: a comprehensive review. *Front. Vet. Sci.* 8, 623800.
- Wang, R., Yang, M., Li, G., Wang, X., Zhang, Z., Qiao, H., Chen, J., Chen, Z., Cui, X., Li, J., 2019. Paclitaxel-betulinic acid hybrid nanosuspensions for enhanced anti-breast cancer activity. *Colloids Surf. B: Biointerfaces* 174, 270–279.
- Wang, W., Zhang, Q., Zhang, M., Lv, X., Li, Z., Mohammadniaei, M., Zhou, N., Sun, Y., 2021. A novel biodegradable injectable chitosan hydrogel for overcoming postoperative trauma and combating multiple tumors. *Carbohydr. Polym.* 265, 118065.
- Wu, B., Liu, D.A., Guan, L., Myint, P.K., Chin, L., Dang, H., Xu, Y., Ren, J., Li, T., Yu, Z., Jabban, S., Mills, G.B., Nukpezah, J., Chen, Y.H., Furth, E.E., Gimotty, P.A., Wells, R. G., Weaver, V.M., Radhakrishnan, R., Wang, X.W., Guo, W., 2023. Stiff matrix induces exosome secretion to promote tumour growth. *Nat. Cell Biol.* 25 (3), 415–424.
- Xia, X., Wang, L., Zhang, X., Wang, S., Lei, L., Cheng, L., Xu, Y., Sun, Y., Hang, B., Zhang, G., Bai, Y., Hu, J., 2018. Halofuginone-induced autophagy suppresses the migration and invasion of MCF-7 cells via regulation of STMN1 and p53. *J. Cell. Biochem.* 119 (5), 4009–4020.
- Xia, D.L., Xu, P.P., Luo, X.Y., Zhu, J.F., Gu, H.Y., Huo, D., Hu, Y., 2019. Overcoming hypoxia by multistage nanoparticle delivery system to inhibit mitochondrial respiration for photodynamic therapy. *Adv. Funct. Mater.* 29, 1807294.
- Xiong, Y., Wang, T., Liu, L., Kou, Y., Zhao, Z., Yuan, M., Chen, Y., Wang, D., Song, S., 2023. Hydrogelation of TPGS for locoregional combination therapy of cancer. *Chem. Eng. J.* 451, 138889.
- Yang, G., Wang, Q.Y., Gao, Y.D., Yang, C.C., Hu, L.D., 2018. Combination of coating and injectable hydrogel depot to improve the sustained delivery of insulin. *J. Drug Deliv. Sci. Technol.* 45, 415–421.
- Yao, Y., Zhao, Z., He, J., Ali, B., Wang, M., Liao, F., Zhuang, J., Zheng, Y., Guo, W., Zhang, D.Y., 2023. Iridium nanozyme-mediated photoacoustic imaging-guided NIR-II photothermal therapy and tumor microenvironment regulation for targeted eradication of cancer stem cells. *Acta Biomater.* 172, 369–381.
- Ye, P., Rodriguez, F.H., Kanaly, S., Stocking, K.L., Schurr, J., Schwarzenberger, P., Oliver, P., Huang, W., Zhang, P., Zhang, J., Shellito, J.E., Bagby, G.J., Nelson, S., Charrier, K., Peschon, J.J., Kolls, J.K., 2001. Requirement of interleukin 17 receptor signaling for lung CXC chemokine and granulocyte colony-stimulating factor expression, neutrophil recruitment, and host defense. *J. Exp. Med.* 194 (4), 519–527.
- Zhang, L., Abbaspourrad, A., Parsa, S., Tang, J., Cassiola, F., Zhang, M., Tian, S., Dai, C., Xiao, L., Weitz, D.A., 2020. Core-Shell nanohydrogels with programmable swelling for conformance control in porous media. *ACS Appl. Mater. Interfaces* 12 (30), 34217–34225.
- Zhang, Z., Li, A., Min, X., Zhang, Q., Yang, J., Chen, G., Zou, M., Sun, W., Cheng, G., 2021. An ROS-sensitive tegafur-PpIX-heterodimer-loaded in situ injectable thermosensitive hydrogel for photodynamic therapy combined with chemotherapy to enhance the tegafur-based treatment of breast cancer. *Biomater. Sci.* 9 (1), 221–237.
- Zhang, G., Lei, Y.M., Li, N., Yu, J., Jiang, X.Y., Yu, M.H., Hu, H.M., Zeng, S.E., Cui, X.W., Ye, H.R., 2022. Ultrasound super-resolution imaging for differential diagnosis of breast masses. *Front. Oncol.* 12, 1049991.
- Zhang, R., Liu, Q., Zhou, S., He, H., Zhao, M., Ma, W., 2023a. Mesenchymal stem cell suppresses the efficacy of CAR-T toward killing lymphoma cells by modulating the microenvironment through stanniocalcin-1. *Elife.* 12, 1–17.
- Zhang, L., Xie, Y., Liang, X., Yin, L., He, C., Yin, Z., Yue, G., Zou, Y., Li, L., Song, X., Tang, H., 2023b. Synthesis of structurally diverse derivatives of aconitine-type diterpenoid alkaloids and their anti-proliferative effects on canine breast cancer cells. *Bioorg. Chem.* 135, 106501.
- Zhao, J., Shi, Y., Cao, G., 2023. The application of single-cell RNA sequencing in the inflammatory tumor microenvironment. *Biomolecules*. 13 (2), 344.
- Zuo, R.N., Zhang, J.J., Song, X.H., Hu, S.H., Gao, X.G., Wang, J.Q., Ji, H., Ji, C.L., Peng, L., Si, H.B., Li, G.H., Fang, K., Zhang, J.R., Jiang, S.X., Guo, D.W., 2021. Encapsulating halofuginone hydrobromide in TPGS polymeric micelles enhances efficacy against triple-negative breast cancer cells. *Int. J. Nanomedicine* 16, 1587–1600.
- Zuo, R.N., Zhang, Y., Chen, X.R., Hu, S.H., Song, X.H., Gao, X.G., Gong, J.H., Ji, H., Yang, F.Z., Peng, L., Fang, K., Lv, Y.J., Zhang, J.R., Jiang, S.X., Guo, D.W., 2022. Orally administered halofuginone-loaded TPGS polymeric micelles against triple-negative breast cancer: enhanced absorption and efficacy with reduced toxicity and metastasis. *Int. J. Nanomedicine* 17, 2475–2491.